Cell – ECM interactions play distinct and essential roles at multiple stages during the development of the aortic arch

Michael Warkala[1,2, §], Dongying Chen[3, §, ¥], Ali Jubran[3, †], AnnJosette Ramirez[1,4, †], Michael Schonning[1,4], Xia Wang[†], Huaning Zhao[1], and Sophie Astrof[1, 2, 4, *].

1. Department of Cell Biology and Molecular Medicine, New Jersey Medical School, Rutgers Biomedical and Health Sciences, Newark, NJ, USA

2. Multidisciplinary Ph.D. Program in Biomedical Sciences: Molecular Biology, Genetics, and Cancer Track, New Jersey Medical School, Rutgers Biomedical and Health Sciences, Newark, NJ, USA

3. Graduate Program in Cell & Developmental Biology, Thomas Jefferson University, Philadelphia, PA, USA

4. Multidisciplinary Ph.D. Program in Biomedical Sciences: Cell Biology, Neuroscience and Physiology Track, New Jersey Medical School, Rutgers Biomedical and Health Sciences, Newark, NJ, USA

¥ Current address: Yale Cardiovascular Research Center, Department of Internal Medicine, Yale University School of Medicine, New Haven, CT 06511, USA.

‡ Current address: Department of Anatomy, Histology & Developmental Biology, School of Basic Medical Sciences, Shenzhen University Health Science Center, Shenzhen, China

§ These individuals contributed equally to the manuscript as co-first authors

† These individuals contributed equally to the manuscript as co-second authors

Short title: Integrin $\alpha5\beta1$ and Fn1 in arch artery formation

* Corresponding author: Sophie Astrof,

sophie.astrof@rutgers.edu

185 South Orange Ave,

Medical Sciences Building, Room I-518,

Newark, NJ, 01703

Total word count: 7746

Subject Codes: Animal Models of Human Disease; Mechanisms; Vascular Biology;

Rationale: Defects in the morphogenesis of the 4th pharyngeal arch arteries (PAAs) give rise to lethal birth defects. Understanding genes and mechanisms regulating PAA formation will provide important insights into the etiology and treatments for congenital heart disease.

Objective: Cell-ECM interactions play essential roles in the morphogenesis of PAAs and their derivatives, the aortic arch artery (AAA) and its major branches; however, their specific functions are not well-understood. Previously, we demonstrated that integrin $\alpha5\beta1$ and fibronectin (Fn1) expressed in the *Isl1* lineages regulate PAA formation. The objective of these studies was to investigate cellular mechanisms by which integrin $\alpha5\beta1$ and Fn1 regulate AAA morphogenesis.

Methods and Results: Using temporal lineage tracing, whole-mount confocal imaging, and quantitative analysis of the second heart field (SHF) and endothelial cell (EC) dynamics, we show that the majority of PAA EC progenitors arise by E7.5 in the SHF and populate pharyngeal arch mesenchyme between E7.5 and E9.5. Consequently, SHF-derived ECs in the pharyngeal arches become organized into a uniform plexus of small blood vessels, which becomes remodeled into the PAAs between 31 – 35 somites. The remodeling of the vascular plexus is orchestrated by signals dependent on pharyngeal ECM microenvironment extrinsic to the endothelium. Conditional ablation of integrin $\alpha5\beta1$ or Fn1 in the Isl1 lineages showed that signaling by the ECM regulates AAA morphogenesis at multiple steps: 1) the recruitment of the SHF-derived ECs into the pharyngeal arches, 2) the remodeling of the uniform EC plexus in the 4th arches into the PAAs; and 3) differentiation of neural crest-derived cells abutting the PAA endothelium into vascular smooth muscle cells.

Conclusions: PAA formation is a multi-step process entailing dynamic contribution of SHF-derived ECs to pharyngeal arches, the remodeling of endothelial plexus into the PAAs, and the remodeling of the PAAs into the AAA and its major branches. Cell-ECM interactions regulated by integrin $\alpha5\beta1$ and Fn1 play essential roles at each of these developmental stages.

Key Words: integrin $\alpha5\beta1$, fibronectin, second heart field, endothelial progenitor cells, pharyngeal arch arteries, aortic arch arteries

Nonstandard Abbreviations and Acronyms in the Alphabetical Order: AAA – aortic arch artery; CHD – congenital heart disease; ECs – endothelial cells; Fn1 – fibronectin; IAA-B – interrupted aortic arch type B; Itga5 – integrin $\alpha5$; PAA – pharyngeal arch arteries; RERSA – retro-esophageal right subclavian artery; SHF – second heart field; VEGFR2 – vascular endothelial growth factor receptor 2

Introduction

Aortic arch artery (AAA) and its major branches comprise an asymmetrical vascular tree that routes oxygenated blood from the heart into the systemic circulation [1]. Defects in the development of the AAA cause devastating forms of congenital heart disease (CHD) due to interruption(s) in the aortic arch, of which interrupted aortic arch type B (IAA-B) is more prevalent [2, 3]. Non-lethal defects in aortic arch morphogenesis such as vascular rings can impact the quality of life by causing constriction of the trachea and esophagus, and resulting in difficulties with eating, breathing, and also in dizziness, vertigo, or tinnitus [4].

The AAA and its major branches develop from the remodeling of three bilaterally symmetrical pairs of pharyngeal arch arteries (PAA), numbered 3, 4, and 6 [5]. It is important to note that phenotypically identical AAA defects arise due to either defects in PAA formation or defects in the remodeling of initially well-formed, symmetrical PAAs into asymmetric AAAs [6]. PAAs arise by vasculogenesis from endothelial precursors originating in the lateral plate mesoderm, also known as the second heart field (SHF) [7-13]. Experiments in zebrafish and mice have demonstrated that PAA formation is a multi-stage process that entails endothelial specification in the SHF, migration of SHF-derived endothelial progenitors into the pharyngeal region, differentiation into ECs, and the assembly of SHF-derived ECs into a plexus of small blood vessels [9, 13-16]. Thereafter, the pharyngeal endothelial plexus becomes connected with the ventral and dorsal aortae. The endothelium of the ventral aortae also forms by vasculogenesis from SHF-derived progenitors and is contiguous with the cardiac outflow tract and the PAAs [9, 11]. Following pharyngeal arch segmentation, the plexus endothelium within each arch is

rearranged into the PAAs [9]. The 3rd PAA is evident by E9.5, before the 4th and 6th PAAs are formed. By the evening of E10.5, all three symmetrical pairs of PAAs are formed. Defects in the formation of the left 4th PAA lead to IAA-B, which is lethal unless corrected by surgery soon after birth [2]. Following PAA formation, neural crest-derived cells closest to the PAA endothelium differentiate into vascular smooth muscle cells (VSMCs), surrounding the PAA endothelium with a VSMC coat by E12.5 [17-21]. While not essential for PAA formation, the differentiation of neural crest (NC)-derived cells into VSMCs is essential for the stability of the PAAs, and for their eventual remodeling into the asymmetrical AAA and its branches; Defects in NC differentiation in the 4th pharyngeal arch lead to arch artery regression, and IAA-B [19, 20, 22]. In summary, IAA-B results due to either defects in the formation of the left 4th PAA or due to its regression.

Morphogenesis of distinct organs and structures proceeds within niches comprised of distinct complements of extracellular matrix (ECM) proteins, and alterations in ECM microenvironment can severely affect embryogenesis [23-27]. We discovered that the pharyngeal arch microenvironment is enriched in the ECM glycoprotein fibronectin (Fn1) both at the mRNA and protein levels [28]. Fn1 is highly expressed in the pharyngeal endoderm, ectoderm, endothelium, and the second heart field (SHF) mesoderm between E8.5 and E10.5, the period coinciding with PA formation [28, 29]. Between E10.5 and E11.5 Fn1 becomes highly upregulated in the NC-derived cells abutting the 4th PAA endothelium, corresponding with the time these cells differentiate into VSMCs. Our previous studies demonstrated that local depletion of Fn1 in the pharyngeal microenvironment using the Isl1^{Cre} knockin mice or in the NC-derived cells, using a variety of NC-expressing Cre lines, resulted in the IAA-B and RERSA [29,

[30]. However, mechanistically, IAA-B in these mutants had distinct cellular etiology: ablation of Fn1 in using the Isl1^{Cre} knockin mice led to defective formation of the 4th PAAs [29], while the ablation of Fn1 in the NC resulted in the regression of originally well-formed 4th PAAs [31].

Integrins are a major class of transmembrane receptors that engage in signal transduction upon binding ECM proteins. Integrins are heterodimers of α and β chains. There are 18 α and 8 β subunits encoded by mammalian genomes, giving rise to 24 different $\alpha\beta$ combinations [32]. Integrin α5 complexes with integrin β1, forming the integrin $\alpha5\beta1$ heterodimer [33]. Integrin $\alpha5\beta1$ binds the ECM glycoprotein fibronectin (Fn1), and regulates Fn1 assembly *in vivo* [34]. Phenotypes resulting from either global or cell-type-specific ablations of integrin α5 (MGI gene symbol: Itga5) or Fn1 in mice are similar [26, 28, 29, 31, 34-41], indicating that integrin $\alpha5\beta1$ is a major Fn1 signal transducer *in vivo*. Previously, we demonstrated that the expression of integrin $\alpha5\beta1$ and Fn1 in the Isl1 lineages was required for the formation of the 4th PAA and that the deletion of either integrin α5 or Fn1 in using the Isl1^{Cre} knockin strain resulted in IAA-B [29]. To understand the mechanisms by which integrin $\alpha5\beta1$ and Fn1 regulate AAA development, we analyzed SHF and endothelial cell dynamics in integrin $\alpha5^{f/-}$; Isl1^{Cre} and Fn1$^{f/-}$; Isl1^{Cre} mutants during PAA formation and remodeling, spanning embryonic days (E) E9.5 - E11.5 of development. Our studies point to the essential roles of cell-ECM interactions mediated by integrin $\alpha5\beta1$ and Fn1 at multiple stages of PAA formation and remodeling.

Methods

147 **Animals** All experimental procedures were approved by the Institutional Animal Care
148 and Use Committee of Rutgers University and conducted in accordance with the
149 Federal guidelines for the humane care of animals.

150 **Tamoxifen injections** *Isl1*^{MerCreMer} knockin mice [42] and Mef2C-AHF-DreERT2
151 transgenic mice [43] were used for temporal labeling of vascular progenitors in the SHF.
152 Tamoxifen was dissolved either in corn oil or in sesame oil at the concentration of 10
153 mg/ml. Labeling was done by i.p. injection of 300 μl of stock solution into pregnant
154 females at multiple time points specified in the legend to Fig. 1. E0.5 was designated to
155 be as noon on the day when the vaginal plug was found.

156 **Whole Mount Immunofluorescence staining** Labeling with BrdU, TUNEL, and
157 staining with antibodies were performed as described [29], and analyzed using IMARIS
158 (Bitplane, USA) [9, 44]. Detailed procedures for staining, analysis and cell quantification is
159 described in [44].
160
161 **Statistics** Statistical analyses were performed using Prism 8 software version 8.4.3.
162 Specific statistical tests are indicated in figure legends.
163

164 **Results**

165 **SHF contributes harbors PAA progenitors between E7.5 and E9.5.** Previous work
166 from our lab demonstrated that in the mouse, the majority of PAA endothelium is
167 derived from the SHF, derived from either Mef2C-AHF-Cre- or Isl1^{Cre}- expressing
168 mesodermal lineages [9]. To define the temporal window during which the SHF

mesoderm harbors endothelial progenitors of the PAAs, we used *Isl1*^{MerCreMer} knockin mice [42] and Mef2C-AHF-DreERT2 transgenic mice [43] combined with pulses of tamoxifen to lineage-label the SHF mesoderm at different developmental times (Fig. 1). Tamoxifen was injected at discrete time points between E6.75 – E9.75, and embryos were dissected at E10.5 and stained to detect lineage labeling in the pharyngeal arches. Entire pharyngeal regions were imaged using confocal microscopy to quantify the contribution of lineage-labeled cells to the PAA endothelium (Fig. 1, panels A-A2). The expression of VEGFR2 and ERG were used to mark EC cell membrane and nuclei [45]. The labeling of the cardiac outflow tract and the right ventricle using *Isl1*$^{MerCreMer/+}$ mice was evident at all stages tested, indicating that our labeling technique was consistent with previous studies (data not shown) [42]. Myocardial cells derived from the SHF are labeled when tamoxifen is injected as early as E6.5 in *Isl1*^{MerCreMer} knockin mice [42], however no PAA ECs were labeled when tamoxifen was injected at E6.75 in this strain (Fig. 1B) or at E7.25 in Mef2C-AHF-DreERT2 transgenic strain (Fig. 1C), suggesting that PAA EC progenitors arise later in the SHF relative to cardiomyocyte progenitors. The peak labeling of the PAA endothelium occurred when tamoxifen was injected at E7.25 in *Isl1*^{MerCreMer} strain (Fig. 1B) and at E8.0 in Mef2C-AHF-DreERT2 strain (Fig. 1C). While tamoxifen injection into *Isl1*^{MerCreMer} resulted in sparse labeling of PAA ECs, the injection of tamoxifen into Mef2C-AHF-DreERT2 transgenic mice led to the labeling of a much larger proportion of ECs in the PAAs (compare Fig. 1B with Fig. 1C). These differences likely reflect that the MerCreMer transgene is present as a single copy as it is knocked into the *Isl1* locus [42], while Mef2C-AHF-DreERT2 is a transgenic strain containing multiple copies of the Mef2C-AHF-DreERT2 transgene [43]. In addition, the

192 expression of *Is1* is downregulated commensurate with endothelial differentiation [46].
193 Thus, potentially low levels of *MerCreMer* expression in EC precursors could have
194 resulted in low labeling of endothelial progenitors in *Isl1*^{MerCreMer} mice relative to Mef2C-
195 AHF-DreERT2 strain. The difference in the timing of peak EC labeling in the PAAs
196 between *Isl1*^{MerCreMer} and Mef2C-AHF-DreERT2 strains is likely due to the earlier onset
197 of *Isl1* expression compared with the expression of the Mef2C-AHF-DreERT2
198 transgene; in fact, Isl1 regulates the expression of Mef2C and the activation of the
199 Mef2C-AHF enhancer [47, 48]. Correspondingly, our experiments demonstrate that the
200 peak endothelial labeling of PAAs in *Isl1*^{MerCreMer} strain precedes that of Mef2C-Dre-
201 ERT2 strain by 18 hours (compare Fig. 1B with Fig. 1C). Interestingly, the accrual of
202 SHF-derived ECs into the 4th arch continues past E8.5 as more SHF-derived cells are
203 labeled in the 4th PAAs than in the 3rd and 6th when tamoxifen is injected at E8.5 and
204 E9.5 (Fig. 1B1, 1C1). Thus, our labeling experiments show that the SHF mesoderm
205 harbors PAA endothelial progenitors between approximately E7.5 and E9.5 of
206 embryonic development.
207
208 To analyze the contribution of the SHF to the PAA endothelium quantitatively and to
209 compare two mouse strains commonly used to label the SHF, we imaged the entire
210 pharyngeal arch region corresponding to arches 3, 4, and 6, and quantified the
211 proportion of SHF-lineage labeled ECs in the PAAs from E10.5 embryos derived from
212 Isl1^{Cre} knockin and Mef2C-AHF-Cre transgenic lines (Fig. 2). The majority of SHF-
213 derived cells in the pharyngeal arches 3 – 6 are found in the endothelium at 37somites,
214 as seen in sections through the pharyngeal arch region (Fig. 2A – B). Each PAA is

comprised of a similar number of ECs (Fig. 2C). However, there were differences in PAA labeling among embryos isolated from Isl1^{Cre} and Mef2C-AHF-Cre mice (Fig. 2D, E). In the constitutive *Isl1^{Cre}* knockin strain, the SHF contribution to the 3rd and 4th PAA endothelium was 79±6% and 77±10%, respectively, and 57±12% to the 6th PAA (Fig. 2D). While the SHF contribution to the 3rd PAA was 45±8% in Mef2C-AHF-Cre transgenic line, which is significantly different from *Isl1^{Cre}* knockin strain ($p<10^{-5}$, one-way ANOVA with Tukey's correction for multiple testing). The SHF contribution to the PAA endothelium of the 4th and 6th PAAs were similar between the two strains ($p>0.2$, one-way ANOVA with Tukey's correction for multiple testing). The difference in the contribution of the SHF to the 3rd PAA between the two strains likely reflects the earlier onset of Cre expression in the *Isl1^{Cre}* knockin strain relative to Mef2C-AHF-Cre transgenic line [47]. These data suggest that about half of the 3rd PAA progenitors arise and leave the SHF prior to the activation of Mef2C-AHF-Cre. These data also indicate that the deletion of one Isl1 allele, as in the *Isl1^{Cre}* knockin strain, does not impair the contribution of the SHF to the PAA endothelium. In summary, our data show that the 4th PAAs differ from the 3rd and the 6th PAAs in the timing during which SHF cells are added, and differ from the 6th PAA in the proportion of SHF-derived cells.

Cell-ECM interactions mediated by integrin α5β1 specifically regulate the accrual of SHF-derived cells into pharyngeal region. Studies described above together with our previous work [9] have established a framework for the analyses of EC dynamics and their genetic regulation during the morphogenesis of AAA and its major branches. Our previous studies demonstrated that the deletion of either integrin α5 or Fn1 in the Isl1

lineages resulted in the defective formation of the 4th PAAs at E10.5, and consequently, IAA-B and retro-esophageal right subclavian artery (RERSA), in these mutants [29]. IAA-B and RERSA are anomalies resulting from defective morphogenesis of the left and right 4th PAAs, respectively [1, 3]. To determine the mechanisms by which integrin $\alpha5\beta1$ and Fn1 regulate the formation of the 4th PAAs, we analyzed PAA development at distinct stages of embryonic development using whole-mount immunofluorescence followed by quantitative analyses of SHF-derived populations and their dynamics.

PAAs form through the coalescence of pharyngeal arch EC plexus, a network of small blood vessels [9, 10]. All pharyngeal arch ECs are located within the plexus at E9.5. At E10.5 (33 – 34 somite stage), 50% of the 4th arch endothelium is found within the PAA (the vessel surfaced in green in (Fig. 3B, C) and 50% is in the plexus (pink in Fig. 3B, C) [9]. About 50% of integrin $\alpha5^{f/-}$; $Isl1^{Cre}$ mutants have defective 4th PAAs, and consequently, 50% of these mutants develop IAA-B and RERSA [29] . We found that 4th PAA is absent in 50% of mutants at 32 – 34 somites (Fig. 3D – F). Instead, the endothelium in the 4th arches is in the form of a plexus of small blood vessels (marked in pink in Fig. 3E, F). A small 4th PAA eventually formed in these mutants by 36 – 39 somites (Fig. 3J, marked in green in Fig. 3K, L; compare with the 4th PAA surfaced in green in control Fig. 3G-I). Similarly, the formation of the 4th PAA was delayed in $Fn1^{f/-}$; $Isl1^{Cre/+}$ mutants (Sup. Fig. 1). This defect was specific to the 4th PAA, as the 3rd and 6th PAAs formed normally in the mutants (vessels surfaced in white and red in Fig. 3). The incidence of IAA-B and RERSA is 50% in integrin $\alpha5^{f/-}$; $Isl1^{Cre}$ and $Fn1^{f/-}$; $Isl1^{Cre/+}$ mutants, which is the same as the incidence of defective 4th PAAs at E10.5 [29].

Therefore, we further investigated the mechanisms by which integrin $\alpha5\beta1$ and Fn1 regulate the formation of the 4th PAAs.

We hypothesized that the defective formation of the 4th PAAs in our mutants could be due to insufficient EC numbers, defective EC proliferation, or survival. To test these hypotheses, we evaluated total EC numbers in the 4th pharyngeal arches of controls and mutants. To quantify EC number, we stained E10.5 embryos with the antibodies to ERG, a transcription factor enriched in the endothelia and either VEGFR2 or Pecam 1, expressed on EC surface, as described [44]. These experiments showed that integrin $\alpha5^{f/-}$; Isl1^{Cre} and Fn1$^{f/-}$; Isl1$^{Cre/+}$ mutants had decreased total number of ECs in the 4th arches at 32 – 33 somites relative to controls (Fig. 3M and Sup. Fig. 1A-C). Despite this decrease in EC numbers, the size of the 4th arches, the tissues within which PAAs form, was not affected (Fig. 3N). EC proliferation in the 4th arch was also not affected in the mutants (Fig. 3O), and neither was cell survival (Sup. Fig. 2). Thus, EC deficiency in the 4th pharyngeal arches of the mutants was not due to defective cell proliferation or survival. The majority of VEGFR2^{+} cells in the pharyngeal region of E9.5 embryos were labeled with GFP (Sup. Fig. 3A – A2, B – B2), indicating that SHF cells in the pharyngeal region of the mutants were not impaired in the acquisition of EC fate. VEGFR2 is expressed the 4th pharyngeal arch endothelium at E9.5, which is a day earlier than Pecam 1 [10]. To determine whether the maturation of pharyngeal arch ECs was affected in the mutants at E10.5, we co-stained embryos with antibodies to VEGFR2 and Pecam 1. Despite defective 4th PAA formation, all VEGFR2^{+} cells in pharyngeal arches of the mutants also expressed Pecam1 at E10.5 (Sup. Fig. 3C, D,

C1, D1), ruling out maturation as a cause for decreased EC numbers in the 4th pharyngeal arch.

Since the maturation, proliferation, and survival of ECs were not affected in our mutants, we tested the hypothesis that defective recruitment of progenitor cells into the pharyngeal arches was the cause for decreased EC numbers in the 4th arch. As we established before, the majority of PAA endothelium arises from the SHF (Fig. 2D, E and [9], and the accrual of SHF-derived cells into the pharyngeal arches is mostly complete by E9.5 (Fig. 1B-C). To quantify the number of SHF-derived cells in the pharyngeal mesenchyme, we used ROSA$^{nT\text{-}nG}$ reporter mice, in which nuclear localization sequences were fused with tdTomato and EGFP, leading to the expression nuclear-localized EGFP upon Cre-induced recombination. We found that the deletion of integrin α5 in the Isl1 lineages impaired the accrual of SHF cells into the pharyngeal region (Fig. 4A-B), while the accrual of SHF-derived cells into the heart was not affected (Fig. 4C).

Splanchnic mesoderm within the dorsal pericardial wall harbors both cardiac and vascular progenitors. To test whether the deficiency in the pharyngeal SHF-derived mesoderm was due to the decrease in SHF cells numbers in the splanchnic mesoderm, we used IMARIS to surface cells within this region and quantified the number of GFP$^+$ cells (see Sup. Fig. 4 for details on surfacing). These experiments showed that the number of GFP$^+$ cells in the splanchnic mesoderm within the dorsal pericardial wall was similar between controls and mutants (Fig. 4D). Next, we computed the proportion of

GFP$^+$ cells in the pharyngeal mesenchyme or in the heart relative to the number of GFP$^+$ cells in the splanchnic mesoderm. While the latter ratio was not affected in the mutants (Fig. 4E), the former was significantly decreased in the mutants (Fig. 4F), suggesting that there is a defect either in the specification of pharyngeal progenitors in the SHF or in their exit from the SHF. Taken together, these experiments indicate that ECM microenvironment sensed through the signaling by integrin $\alpha5\beta1$ is important for the accrual of the SHF-derived mesoderm to the pharyngeal arches (Model in Fig. 8, PAA formation panel A1).

Integrin $\alpha5\beta1$ and fibronectin regulate the remodeling of pharyngeal plexus into the 4th PAAs independently of EC numbers. Interestingly, the number of SHF-derived cells and ECs in the mutants recovered by the 34-35 somite stage, and was similar to that of controls (Fig. 5A). Total number of GFP$^+$ cells also recovered (Fig. 5B). The percentage of GFP$^+$ ECs in the pharyngeal arches of controls and mutants were comparable (Fig. 5C), indicating that the recovery was not due to the recruitment of ECs from an alternative mesodermal source. The recovery of pharyngeal EC numbers was likely mediated through the proliferation of SHF-derived ECs. The basis for this conclusion is the following. The proliferation index of pharyngeal arch ECs was unaltered in the mutants (Fig. 3O), and the proliferation index of ECs in the pharyngeal plexus is 2-fold higher than that of PAA ECs, both in controls and in mutants (Fig. 3O, plexus). Since the proportion of ECs in the pharyngeal plexus is higher in the mutants than in controls (Sup. Fig 1D), the higher proliferation index of plexus ECsin the mutants is likely responsible for EC recovery. Our quantitative analyses indicate that PAA

formation phenotypes in integrin $\alpha5^{f/-}$; $Isl1^{Cre/+}$ and $Fn1^{f/-}$; $Isl1^{Cre/+}$ mutants are indistinguishable from one another (Sup. Fig. 1), suggesting that integrin $\alpha5\beta1$ is a major receptor transducing Fn1 signals within the pharyngeal microenvironment.

Despite the recovery of EC numbers (Fig. 5A), PAAs remained thin in integrin $\alpha5^{f/-}$; $Isl1^{Cre}$ and $Fn1^{f/-}$; $Isl1^{Cre/+}$ mutants (Fig. 3G – L), and there was 2 – 3-fold decrease in the proportion of pharyngeal arch ECs in the 4th PAAs at all stages analyzed at E10.5 (Fig. 6A). The size of the 4th PAA increases between 32 – 39 somites, as more ECs are added to the PAA from the plexus (Sup. Fig. 5), and is reflected in the percent of pharyngeal arch ECs in the PAA [9]. In controls, plexus ECs in the 4th arch begin coalescing into the PAA when embryos reach between 31 and 32 somites [9] (Sup. Fig. 5). These rearrangements result in an initially thin 4th PAAs, in which approximately 50% of the pharyngeal arch ECs are in the plexus and 50% in the PAA at 32 – 34 somite stage [9]. As the development proceeds, by 36-39 somite stage, > 60% of the 4th pharyngeal arch endothelium becomes incorporated into the 4th PAA [9]. Thus, the percentage of the pharyngeal arch endothelium in the 4th PAA can be taken as a measure of PAA formation. The higher the proportion, the larger the PAA [9].

To understand the mechanisms by which integrin $\alpha5\beta1$ and Fn1 regulate the remodeling of the uniform endothelial plexus into the PAA in the 4th arch, we examined EC dynamics in control and mutant embryos at three time points, corresponding with 32 – 33 somites, 34 – 35 somites, and 36 – 39 somites. These stages span about 6 hours on the 10th day of mouse embryonic development. The formation of the 4th PAAs lagged in mutants relative to controls at all time points tested during E10.5 (Fig. 6A and Sup Fig. 1D, E), and 7 of the 16 embryos analyzed contained only a plexus of ECs and

lacked the 4th PAAs at the 32 – 34 somite stage (Sup. Fig. 1E), a stage at which over 50% of the 4th arch endothelium in controls is located within the 4th PAAs [9] (Fig. 6A and Sup Fig. 1E).

Since mutant embryos had fewer ECs in the 4th pharyngeal arches compared with controls prior to the 36th somite stage, we performed correlation analyses to test the hypothesis that the formation of the 4th PAAs depended on the total EC number or EC density in the 4th pharyngeal arches. As described above, the percentage of pharyngeal arch ECs in the PAA relative to the plexus can be taken as a measure of PAA formation (Sup. Fig. 5) [9]. Thus, for these analyses, we quantified EC numbers in control embryos isolated between 32 to 39 somite stages and plotted them against the percent of ECs in the 4th PAAs (Fig. 6B). Despite the sharp, over a 3-fold increase in the number of ECs in the 4th arches between these stages [9], the formation of the 4th PAAs was independent of the total EC number in the 4th pharyngeal arch tissue (Fig. 6B) or EC density (Fig. 6C) in controls throughout the 10th day of embryonic development. Similarly, correlation analysis of PAA formation in the mutants with defective (thin) and normal 4th PAAs, showed that similar to controls, the rearrangement of plexus ECs into the PAA did not depend on the number of total number of ECs in the 4th pharyngeal arches of mutants (Fig. 6D).

Next, we compared PAA formation in controls and mutants that had a similar number of ECs in the 4th pharyngeal arches (Fig. 6E). These analyses showed that in groups of mutant and control embryos with a similar number of ECs, the percent of ECs in the PAAs was lower in the mutants (boxes in Fig. 6E). These data indicate that the reorganization of the plexus ECs into the PAA in the 4th pharyngeal arch does not

374 depend on the EC number at E10.5, and is regulated by factors extrinsic to the
375 pharyngeal arch endothelium. In summary, our studies indicate that during the 10th day
376 of embryonic development, cell – ECM interactions mediated by integrin α5β1 and Fn1
377 are essential for the remodeling of the initially uniform vascular plexus into the PAA in
378 the 4th pharyngeal arches (Model in Fig. 8, PAA formation panel A2).

379

380 **The expression of integrin α5 in the Isl1 lineage is required for the differentiation**
381 **of neural crest cells into vascular smooth muscle cells.**

382 In the Tbx1$^{+/-}$ mouse model of 22q11 deletion syndrome, PAA formation recovers in 50
383 – 68% of the mutant mice [49, 50]. To determine whether the rearrangement of the
384 endothelial plexus in the 4th arch was blocked or delayed, we examined E11.5 embryos.
385 The incidence of IAA-B and RERSA in integrin α5$^{f/-}$; Isl1^{Cre} mutants is 50%, which is the
386 same as the incidence of defective 4th PAA formation. Therefore, we expected to find
387 absent or thin 4th PAAs in the mutants at E11.5. Contrary to our expectations, the
388 formation of the 4th PAAs recovered in the mutants by E11.5, and PAA perimeters in the
389 mutants were comparable with controls (Fig. 7A, n=8). Consistent with the recovery of
390 SHF-derived ECs numbers by 33 – 35s, PAA ECs were GFP^{+} cells in the mutants as in
391 controls (compare Fig. 7C1 with 7D1, arrowheads). Regression of left 4th PAAs results
392 in IAA-B and regression of the right 4th results in RERSA [51, 52]. Since 50% of *integrin*
393 *α5$^{flox/-}$; Isl1^{Cre}* mutants develop 4th arch artery defects, such as IAA-B and RERSA [29],
394 these data indicated that the 4th PAAs eventually regress in the mutants. Arch artery
395 regression is commonly caused by the defective differentiation of neural crest cells

surrounding the PAA endothelium into vascular smooth muscle cells, VSMCs [52-57]. In pharyngeal arches, VSMCs exclusively arise from NC-derived cells [49, 58, 59]. To determine whether the differentiation of NC-derived cells into VSMCs was affected in our mutants, we analyzed VSMC differentiation in the pharyngeal arches. For these experiments, we calculated the fraction of vessel perimeter covered by alpha smooth muscle actin (αSMA)-expressing cells, using previously-developed methodology [31]. We found that the differentiation of NC-derived cells into VSMCs was severely diminished around the PAAs in the mutants (quantified in Fig. 7B; compare sections in Fig. 7C, D, magnified in Fig. 7C2, D2; zoom-out panels are in Sup. Fig. 6). The decrease in αSMA expression was not due to NC cell death (Sup. Fig. 2).

Even though, the *Isl1* lineage marks a subset NC-derived cells [60], Isl1 protein is not expressed in NC-lineage cells in the pharyngeal arches, and Isl1 lineage does not label cells adjacent to the PAA endothelium (Fig. 7C1, D1) [29]. Moreover, comparison of NC lineage (Fig. 7E – E4) and Isl1 lineage maps at E11.5 demonstrates that αSMA expression coincides with the NC lineage (Fig. 7E2), but not with Isl1 lineage-labeled cells (arrows in Fig. 7C1 and C2 point to αSMA-expressing cells; arrowheads point to GFP^+ PAA endothelium). These studies indicate that the expression of integrin α5 in the Isl1 lineage(s) regulates the differentiation of NC cells into VSMCs in a non-cell autonomous manner. These results are consistent with our previous experiments demonstrating that the expression of integrin α5 in the *Mesp1* lineage marking the anterior mesoderm regulates the differentiation of NC cells into VSMCs around the 4^{th} PAA [59]. Since the deletion of integrin α5 in the *Mesp1* lineage does not result in defective or delayed PAA formation [59], these data taken together, indicate that the

419 defect in VSMC differentiation in *integrin $\alpha5^{flox/-}$; Isl1^{Cre}* mutants is not merely due to the
420 delayed accrual of arch artery endothelium, or delayed remodeling of the vascular
421 plexus into the PAA. In summary, our studies also indicate that in addition to regulating
422 4th PAA formation, integrin α5 expressed in the *Isl1* lineages plays an independent role
423 in arch artery morphogenesis, namely in the differentiation of NC-derived cells into
424 VSMCs (Fig. 8A).

425 The differentiation of NC into VSMCs is orchestrated in part by a relay of Notch
426 signaling transduced from the PAA endothelium to the surrounding layers of NC-derived
427 cells [56]. The activation of Notch signaling in the NC is required for the differentiation of
428 NCs into VSMCs [52, 56]. We demonstrated that this pathway was regulated by the
429 expression of integrin α5 and fibronectin specifically by NC-derived cells at E11.5 [31]. To
430 test the possibility that the expression of integrin α5 in the *Isl1* lineages regulates the
431 lateral propagation of Notch from the PAA endothelium to the adjacent NC-derived cells,
432 we stained control and mutant sections with an antibody to Notch Intracellular Domain
433 (NICD), an activated form of Notch. However, Notch signaling was activated
434 comparably in controls and mutants, despite the severe deficiency in the differentiation
435 of NC cells into VSMCs in the mutants (compare Fig. 7C2 – C4 with Fig. 7D2 – D4,
436 arrows). These experiments indicate that the expression of integrin α5 in the pharyngeal
437 arch mesoderm regulates the differentiation of NC cells into VSMCs independently of
438 Notch. Furthermore, these experiments indicate that while the activation of Notch is
439 necessary for the differentiation of NC-derived cells into VSMCs, it is not sufficient.
440 Taken together, with our previous work [31, 59], studies in this manuscript demonstrate that

cell-ECM interactions regulated by integrin α5β1 and Fn1 play multiple, pleiotropic, and stage-specific functions during the morphogenesis of the 4th PAAs (Fig. 8).

Combinatorial expression of integrin α5 and fibronectin from multiple lineages in the pharynx regulates the formation of the 4th PAAs.

The *Isl1* lineages encompass the mesoderm in the SHF and pharyngeal arches, pharyngeal endoderm, surface ectoderm, and some NC-derived cell populations, although not the NC in the pharyngeal arches [29, 42, 59, 60]. Our previous studies indicated that the combined expression of integrin α5β1 or Fn1 in the surface ectoderm and the NC was not required for the formation of the 4th PAAs [29, 31]. However, even though PAA formation occurred normally in these mice, the 4th PAAs regressed later due to defects in the differentiation of NC-derived cells into VSMCs, resulting in RERSA and IAA-B [31] (Fig. 8). The expression of either integrin α5β1 or Fn1 in the SHF lineage marked by the expression of the Mef2C-AHF-Cre transgene is also not required for PAA formation (Sup. Tables 1 and 2), indicating that the expression of integrin α5β1 or Fn1 in the SHF alone is not required for cardiovascular development. Consistent with these findings, the expression of integrin α5β1 in the *Mesp1* lineage or in the endothelium was not required for PAA formation [59, 61] (Fig. 8). Instead, the expression of integrin α5β1 in the Mesp1 lineage was required for PAA stability, and the deletion of integrin α5 in *Mesp1* lineage which includes the PAA endothelium resulted in IAA-B and RERSA (Fig. 8) [59, 61].

The difference in the phenotypes resulting from the deletion of integrin α5 using Mef2C-AHF-Cre and $Mesp1^{Cre}$ are likely the result of differences in the timing of Cre expression (e.g. the later onset of Mef2C-AHF-Cre may have allowed the perdurance of integrin

463 α5β1 protein through the stages where it's required for mesoderm-NC interactions).
464 Alternatively, the expression of integrin α5β1 in Mesp1 lineage-derived mesodermal
465 cells prior to E8.5 is important for the regulation of NC cell fate in the pharyngeal arches
466 [59].

467 Lastly, we tested whether the expression of integrin α5 in the endoderm regulated PAA
468 formation. For these experiments, we used the constitutive Sox17$^{2A\text{-}iCre}$ knockin mouse
469 line, in which Cre is expressed in the endoderm and pharyngeal arch ECs (Sup. Fig. 7A
470 – A4) [62]. However, PAAs formed normally in *α5$^{flox/-}$;* Sox17$^{2A\text{-}iCre}$ mutants (Sup. Fig. 7B,
471 B1, C, C1). Together, these data indicate that combinatorial expression of integrin α5
472 and Fn1 in the Isl1 lineages is necessary for the proper formation of the 4th PAAs (Fig.
473 8).

474

475 **Discussion**

476 Proper development of the 4th PAAs is central to the ability of a newborn to survive and
477 thrive (Karunamuni et al., 2014; Moon, 2008). The formation of the 4th pair of the PAAs
478 is regulated by a number of genes including *Tbx1, Pax9, Gbx2, Fgf8, Crkl, PlexinD1,*
479 *and Nrp1*, e.g., [63-67]. However, cellular mechanisms by which these genes mediate PAA
480 formation are not well-understood. Unraveling the dynamics of EC progenitors and their
481 descendants during PAAs formation is vital to understanding the genetic and cellular
482 mechanisms regulating PAA formation and how they are altered in congenital heart
483 disease.

In this manuscript, we have demonstrated that the SHF is the primary source of the PAA endothelium and that the majority of endothelial progenitors giving rise to the PAAs are already present in the SHF by E7.5. PAA progenitors exit the SHF and contribute to the PAAs over a span of about 2 days, from E7.5 to E9.5.

Lineage labeling using constitutive Cre lines Isl1^{Cre} and Mef2C-AHF-Cre led to similar labeling of the PAA endothelium, with the exception of the 3rd PAA, which is labeled 50% more efficiently when Isl1^{Cre} line of mice is used. This difference likely reflects the timing of Cre expression in Isl1^{Cre} and Mef2C-AHF-Cre strains, with Mef2C-AHF-Cre lagging by about a day [42, 48, 68]. The difference in the labeling efficiency suggests that about half of the endothelial progenitors of the 3rd PAAs have exited the SHF by the time Mef2C-AHF-Cre is expressed. Our fate mapping studies show that there are differences in the timing and the extent of SHF contribution to the PAAs. In particular, if one were to use Mef2C-AHF-Cre to generate mutations, the 4th PAAs could be more affected than the 3rd and the 6th because in the MEf2C-AHF-Cre strain, the contribution of the SHF lineage-labeled ECs to the 4th PAA endothelium is the highest.

By using whole-mount imaging and quantitative analyses of EC populations in the pharyngeal arches, we previously demonstrated that the morphogenesis of the 4th PAAs occurs gradually throughout the 10th day of the embryonic development and entails a rapid accumulation of ECs: endothelial population in the 4th pharyngeal arch increases more than three-fold in about eight hours of development, from 30 – 39 somites [9]. This

505 steep increase is unlikely to occur solely due to EC proliferation, and our labeling
506 experiments show that SHF-derived cells are still being added to the 4th PAA after E9.5.

507 Our studies show that integrin $\alpha5\beta1$ and Fn1 are important for initial recruitment of SHF-
508 derived ECs into the 4th pharyngeal arches, and that in the absence of integrin $\alpha5$ or
509 Fn1 in the Isl1 lineages results in EC deficiency up to 32 – 34 somite stage. Despite the
510 initial EC deficiency in the 4th arch, EC numbers recover in integrin $\alpha5^{f/-}$; Isl1$^{Cre/+}$ and
511 Fn1$^{f/-}$; Isl1$^{Cre/+}$ mutants by the 34 – 35 somite stage. We demonstrate that the recovery
512 of EC cell numbers in the pharyngeal arches is not due to compensation from an
513 alternative endothelial source. Instead, we show that the proliferation index of plexus
514 endothelium is 2-fold higher than that of ECs in the 4th PAA (Fig. 3O). This difference in
515 the proliferation index is maintained in the mutants (Fig. 3O). We hypothesize that since
516 the majority of ECs is in the plexus at 32 – 33 somites in the mutants, their proliferative
517 advantage over ECs in the PAA allows the EC number in the mutant arches to recover
518 by the end of E10.5.

519 In spite of the recovery of EC populations in the 4th arches, the 4th PAAs were either thin
520 or absent in 50% of all the 4th arches by 36 – 39 somite stages [29]. Our regression
521 analysis showed that the rearrangement of the 4th pharyngeal arch ECs into the PAA
522 was not dependent on the number or density of ECs in the 4th arch. These data suggest
523 that the remodeling of the uniform endothelial plexus into the PAA in the 4th arch is
524 mediated by factors extrinsic to the endothelium. The disruption of the remodeling in our
525 mutants indicates an essential role for cell – ECM interactions in this process.

526

The *Isl1* lineage encompasses multiple cell types within the pharynx including pharyngeal epithelia, mesoderm, and a population of NC cells in the cardiac outflow tract [60, 68]. Pharyngeal endoderm and the ectoderm are important signaling centers regulating intercellular communications among the germ layers composing the arches during the morphogenesis of cardiopharyngeal organs and structures [27, 69, 70]. Modulation of the extracellular microenvironment within the pharynx is essential for the development cardiovascular system [29, 31, 59, 63, 64, 71-81]. The expression of *Fn1*, an essential ECM glycoprotein, is highly enriched in the pharyngeal epithelia [28, 29], and our studies show that signaling by Fn1 in the Isl1 lineages is important for the accrual of SHF-derived cells to the pharyngeal mesenchyme, and for the formation of the 4th PAAs. In the latter step, signaling by Fn1 in tissues extrinsic to the pharyngeal arch endothelium regulates the remodeling of endothelial plexus into the PAA in the 4th arch. While Fn1 expression in the NC regulates PAA stability after the 4th PAA has formed [29, 31] (Fig. 8).

In this manuscript, we investigated the tissues wherein signaling by Fn1 is important for PAA formation. Integrin $\alpha5\beta1$ is a major Fn1 receptor during embryogenesis [28-30, 34, 38, 39, 41], and the deletion of integrin $\alpha5$ or Fn1 in the Isl1 lineages results in identical phenotypes [29]. To determine the cell type(s) in which signaling by Fn1 regulates PAA formation, we ablated integrin $\alpha5$ in each of the tissues comprising Isl1 lineage individually or in combination. The deletion of integrin $\alpha5$ in the SHF (Mef2C-AHF-Cre strain), the entire anterior mesoderm (Mesp1^{Cre}), the NC (Wnt1-Cre2, P3Pro-Cre), the

549 NC and surface ectoderm (TFAP2α^{IresCre}), or the endoderm and endothelia (Sox17^{2A-}
550 ^{iCre}) resulted in normal PAA formation (this study and [29, 31, 59]). Therefore, we conclude
551 that combinatorial signaling by integrin α5β1 from pharyngeal endoderm, mesoderm,
552 and the surface ectoderm is essential to mediate the formation of the 4th PAAs. While
553 signaling in the mesoderm and the neural crest is important for PAA stability (Fig. 8).

554

555 The PAAs form within the neural crest-derived pharyngeal mesenchyme and the PAA
556 endothelium induces the differentiation of the adjacent NC-derived cells into VSMCs [56].
557 Despite the initial delay in the formation of the 4th PAAs, the size of PAAs in integrin α5$^{f/-}$
558 ; Isl1$^{Cre/+}$ mutants recovers by E11.5. At this time, we observed a profound deficiency in
559 the expression of αSMA by NC-derived cells around the PAAs in the mutants.
560 Deficiency in VSMC differentiation causes vessel regression [31, 52, 57, 82, 83], consistent
561 with our finding that integrin α5$^{f/-}$; Isl1$^{Cre/+}$ and Fn1$^{f/-}$; Isl1$^{Cre/+}$ mutants develop IAA-B and
562 RERSA; defects that are caused by the aberrant morphogenesis of the left and right 4th
563 PAAs, respectively [29]. Our previous studies using integrin α5$^{f/-}$; Mesp1$^{Cre/+}$ mice
564 demonstrated that the expression of integrin α5 in the mesoderm regulates NC
565 differentiation into VSMCs without affecting PAA formation, and integrin α5$^{f/-}$; Mesp1$^{Cre/+}$
566 mice develop IAA-B and RERSA [59] (Fig. 8). Thus, the roles of integrin α5β1 and Fn1 in
567 the formation of the 4th PAAs are separate from their roles in the differentiation of NC-
568 derived cells into VSCMs [31].

569

570 Mechanisms that lead to IAA-B are complex but generally arise due to either of the
571 following two broad categories of defects: a) defects in the formation of the left 4th PAA
572 or b) defects in the stability of an otherwise well-formed 4th PAA. NC ablation studies in
573 chick and genetic manipulation of the neural crest demonstrate that NC is not required
574 for PAA formation [51, 52]. Even in the extreme case of neural crest ablation, PAAs form [51].
575 However, defective differentiation of NC-derived cells into VSMCs leads to PAA
576 regression resulting in various malformations in the aortic arch and its branches,
577 including IAA-B and RERSA [31, 52, 82]. Our studies show that the expression of integrin
578 $\alpha 5\beta 1$ in the pharyngeal mesoderm and the NC are required for NC-to-VSMC
579 differentiation, and the expression of integrin $\alpha 5\beta 1$ in either of these lineages alone is
580 not sufficient for this process [31, 59].
581

582 Defects in the formation of the 4th PAAs often occur in conjunction with 22q11 deletion
583 syndromes [84]. Cumulatively, four prospective studies found that between 40 and 90% of
584 interrupted aortic arch type B (IAA-B) cases diagnosed in fetuses, neonates, and
585 children can be attributed to deletions in the 22q11 region [85]. Studies using *Tbx1*$^{+/-}$ mice
586 that model 22q11 deletion syndrome indicated that defective formation of the left 4th
587 PAA underlies IAA-B in these patients [65, 86, 87]. Intriguingly, several independent
588 publications demonstrated that *Tbx1* regulates the expression of integrins and
589 extracellular matrix (ECM) components, and showed that defects in cell-ECM
590 interactions downstream of *Tbx1* precede pathological sequelae and cardiovascular
591 defects in *Tbx1* mutants [71-73]. Interestingly, about 50% of Tbx1$^{+/-}$ mice recover from the
592 initial defect in PAA formation, and are viable and fertile [50]; However, this recovery can

be impeded by the reduction in the expression of Fn1 [49]. Thus, alterations in cell-ECM interactions and pharyngeal ECM microenvironment may underlie lethal AAA defects in 22q11 deletion syndrome downstream of *Tbx1*.

The significance of our work lies in the identification of cellular dynamics regulating PAA formation and the intricate temporal and cell-type specific roles of cell-ECM interactions in the regulation of aortic arch morphogenesis at multiple steps of its formation and remodeling (Fig. 8).

Acknowledgements We thank Richard Hynes, Chenleng Cai, Sylvia Evans, Benoit Bruneau, Heicko Lickert, and Hongkui Zeng for the gift of mouse strains, and Brianna Alexander and Nathan Astrof for careful reading of the manuscript.

Sources of Funding This work was supported by the funding from the National Heart, Lung, and Blood Institute of the NIH R01 HL103920, R01 HL134935, and R21 OD025323-01 to SA, and pre-doctoral fellowship F31HL150949 to AJR.

Disclosures None

Supplemental Materials
Expanded Materials & Methods
Online Figures 1 – 7

Figure Legends

Figure legends are also included with the figures

Figure1. Endothelial PAA progenitors are arise in the SHF as early as E7.25. Isl1^{MerCreMer} and Mef2C-AHF-DreERT2 males were mated with the appropriate reporter females (see Methods). E0.5 was considered to be noon on the day of the vaginal plug. Tamoxifen was injected at specified times, embryos were dissected at E10.5, and stained to detect VEGFR2 (blue), ERG (red), or tdTomato (orange). **A.** Sagittal view and 3D reconstruction through the left pharyngeal region. Inset- 3D reconstruction of PAAs. **A1 – A2.** Sagittal optical sections through the embryo shown in **A.** Labeling efficiency was quantified by calculating the ratio of the number of ERG^{+} tdTomato^{+} ECs to the total number of ERG^{+} ECs in PAAs using IMARIS spot function. **B.** Highest labeling of PAA endothelium occurred when tamoxifen was injected at E7.25 in Isl1^{MerCreMer} knockin mice. **B1.** SHF-derived cells continute to be added the 4th PAA after E9.5. C. Peak labeling of PAA ECs occurred when tamoxifen was injected at E8.0 in Mef2C-AHF-DreERT2 strain. **C1.** Injection of tamoxifen at E8.5 led to a more efficient labeling of the 4th PAAs than the 3rd and 6th PAAs.

Figure 2. Majority of PAA ECs are SHF-derived; there are differences in the contribution of the SHF to the PAA endothelium depending on the strain used. Mef2C-AHF-Cre; ROSA^{tdTomato} embryos (35 – 37 somites) were stained with antibodies to VEGFR2 (turquoise) to detect endothelial cells, tdTomato (orange) to detect SHF-derived cells, and DAPI (blue) to stain cell nuclei. **A – A2.** 3D reconstructions of PAAs and their connections with the dorsal aorta (dAo) and the aortic sac (Ao S). **B – B2.**

Sagittal optical sections to show the distribution of all SHF-derived cells in the pharyngeal arches. PAAs 3 – 6 are labeled. Magnifications are the same in all panels. All scale bars are 100 μm. **C.** The number of $VEGFR2^{+}EGR^{+}$ cells in the pharyngeal arches was quantified in 5 E10.5 embryos at 35 – 37 somites using IMARIS. Each dot is one arch. Red line marks the median. Black lines mark quartiles. Differences among the three PAA pairs are not significant, $p>0.1$ by one-way ANOVA with Tukey's correction for multiple testing. **D – E.** The percentage of $VEGFR2^{+}EGR^{+}$ cells expressing the Cre reporter was determined in each PAA (orange bars). Blue bars are the percent of $VEGFR2^{+}EGR^{+}$ cells that were not labeled with the Cre reporter. **D.** The use of constitutive $Isl1^{Cre}$ strain resulted in labeling of more than 80% of ECs in the 3rd and 4th PAAs. **E.** The use of Mef2C-AHF-Cre strain resulted in a significantly higher labeling of the 4th PAAs than the 3rd and the 6th. The difference in the labeling efficiency of 6th PAAs between the two strains was not significant, $p> 0.2$. All statistical analyses were performed using one-way ANOVA with Tukey's correction for multiple testing.

Figure 3. Formation of the 4th PAA is delayed in integrin $\alpha5^{flox/-}$; $Isl1^{Cre}$ mutants. Integrin $\alpha5^{flox/+}$; $Isl1^{Cre}$ control and $\alpha5^{flox/-}$; $Isl1^{Cre}$ mutant embryos were dissected at different somite stages at E10.5 and stained to detect Pecam1. PAAs are numbered and somite stages are indicated in the first row. **A, D, G, J.** 3D reconstructions of whole-mount Pecam 1 staining (light blue). **B, E, H, K.** PAA endothelium in the 3rd, 4th and 6th arches shown in the row above was surface-rendered white, green and red, respectively. In addition, the plexus endothelium in the 4th arch was surface-rendered in pink. **C, F, I, L.** Left side and ventral views of surface-rendered PAAs and the plexus.

Development of the 4th PAAs was specifically affected in the mutants (**E, F**). Magnification is the same in all panels. Scale bar is 100 μm. **M.** Total number of endothelial cells was quantified as described in Methods. Mutants have EC deficiency in the 4th arch as 32 – 33 somites. **N.** The sizes of the 4th arches are comparable between controls and mutants. **O.** EC proliferation in the PAA and the plexus in the 4th arches was similar in controls (C) and mutants (M). In all plots, solid lines mark the median, dashed lines mark the quartiles. Each dot marks one arch. At least 3 mutants and 3 controls were assayed. Statistics were evaluated using 2-tailed, unpaired Student's t test with Welch's correction for unequal standard deviation between samples.

Figure 4. **The expression of integrin a5 in the Isl1 lineages is required for the accrual of SHF-derived cells to the pharyngeal mesenchyme.** Control and mutant embryos carrying one ROSA^{nTnG} reporter allele were dissected at E9.5 (18 – 20 somite stage) and stained with DAPI and anti-GFP antibodies. Whole embryos were imaged and the number of GFP^{+} cells (SHF-derivatives) in the arch mesenchyme, splanchnic mesoderm, and in the heart was quantified as described in Sup. Fig. 4. **A.** The total number of SHF cells in the mesenchyme of the 1st and 2nd arches was decreased in the mutants. **B.** The total number of of GFP^{+} cells in the pharyngeal mesenchyme corresponding with the future arches 3 – 6 was decreased in the mutants. The number of SHF cells in heart (**C**) and the splanchnic mesoderm (**D**) was not affected. **E.** The proportion of GFP^{+} cells in the heart relative to GFP^{+} cells in splanchnic mesoderm was not affected in the mutants. **F.** The proportion of GFP^{+} cells in the posterior pharyngeal mesenchyme relative to the number of GFP^{+} cells in splanchnic mesoderm was

680 significantly decreased in the mutants. Each dot marks one embryo, red lines mark
681 medians, dotted lines mark quartiles; p values were determined using unpaired, 2-tailed
682 Student's t tests.

683

684 **Figure 5. Recovery of EC numbers in integrin $\alpha5^{flox/-}$; $Isl1^{Cre/+}$ mutants. A.** Total EC
685 number has recovered in integrin $a5^{flox/-}$; $Isl1^{Cre/+}$ mutants by the 34th somite stage. **B.**
686 Total number of SHF-derived mesodermal cells has recovered in the pharyngeal arches
687 in integrin $\alpha5^{flox/-}$; $Isl1^{Cre/+}$ mutants by the 34th somite stage. **C.** The fraction of SHF-
688 derived ECs in pharyngeal arches is comparable among control and mutant embryos.
689 This fraction was calculated by quantifying the number of GFP^+ERG^+ cells and dividing
690 by the total number of ERG^+ cells in the entire pharyngeal arches (e.g. ECs in PAA and
691 plexus were quantified). Statistical significance was evaluated using one-way ANOVA
692 with Tukey's correction for multiple testing.

693

694 **Figure 6. Integrin α5b1 and Fn1 regulate the remodeling of EC plexus during the**
695 **formation of the 4th pharyngeal arch arteries. A.** The proportion of ECs in the 4th
696 PAAs in the mutant is significantly lower than in controls at all stages analyzed at E10.5,
697 including the stages when the EC population in the 4th pharyngeal arch has recovered in
698 the mutants; 2-tailed, unpaired Student's t test. **B – C.** Linear regression analyses
699 indicate the absence of linear correlation between the size of the 4th PAA and EC
700 number (**B**) or density (**C**). PAA size is expressed as the percentage of pharyngeal arch
701 endothelial cells in the 4th PAA in control embryos on the y-axis. **D.** Total EC number (x-

axis) from mutants with defective (open symbols) or unaffected 4th PAA (closed symbols) were plotted against the size of the 4th PAAs, y -axis. Regression analysis indicated low correlation between these properties. Circles: 32 – 33 somite embryos, rhombi: 34 – 35 somite embryos, triangles: 36 – 39 somite embryos. **E.** The rearrangement of the endothelial plexus into the 4th PAAs is defective in mutants relative to controls with the same number of endothelial cells in the 4th arch (red boxes). EC – endothelial cell(s). Controls: $\alpha5^{f/+}$; Isl1$^{Cre/+}$ and Fn1$^{f/+}$; Isl1$^{Cre/+}$ embryos; Mutants: $\alpha5^{f/-}$; Isl1$^{Cre/+}$ and Fn1$^{f/-}$; Isl1$^{Cre/+}$ embryos.

Figure 7. The expression of integrin α5β1 in the Isl1 lineages regulates the differentiation of neural crest-derived cells into VSCMs at E11.5 A. PAA perimeter has recovered in size in the mutants by E11.5. **B.** Smooth muscle coverage of the left 4th and left 6th PAA was deficient in the mutants. **C – D**. Despite defective differentiation of NC cells into VSMCs, the activation of Notch in the pharyngeal arch mesenchyme was not altered in the mutants. PAAs are numbered. PAA lumens at E11.5 are derived from the Isl1^{Cre} lineage (green, arrowheads in **C1** and **D1**). αSMA^{+} cells are GFP-negative in Isl1^{Cre} strain (arrows in **C1-C2**). **C2 – D2**. VSMC differentiation assayed by the expression of alpha smooth muscle actin (αSMA, blue) is specifically affected around the 4th PAAs in the mutants (compare regions marked by the arrows in **C2** and **D2**). The activation of Notch assayed by the expression of NICD is not altered in the mutants with defective VSCM differentiation (arrows in **C3, C4** and **D3, D4**). **E.** Fate map using TFAP2α^{IRESCre} shows the location of NC-derived cells in the pharyngeal arches. Note extensive colonization of the mesenchyme between the endodermal pouches (endo) by the TFAP2α^{IRESCre} lineage. **E2**. αSMA^{+} cells are GFP^{+} in

725 TFAP2α^{IRESCre} strain. All scale bars are 50 μm. Additional zoom-out views are in Sup.
726 Fig. 6.

727

728 **Figure 8. Cell – ECM interactions play essential roles at multiple stages during the**
729 **development of the aortic arch and its branches. A.** The expression of integrin α5β1
730 and Fn1 in the Isl1 lineages is required for the formation of the 4th PAAs. **A1**. A
731 schematic of Isl1 lineages (green) in the pharynx at E8.5 – E9.5. Green arrows indicate
732 migration of splanchnic mesoderm cells into the pharyngeal arches. Red lines signify
733 enriched localization of Fn1 protein at germ layer borders. Integrin α5β1 is expressed in
734 all cell types in the pharynx at E8.5 (Chen et al., 2015) and regulates the accrual of
735 pharyngeal mesoderm from the SHF (green arrows). **A2.** During the 10th day of mouse
736 development, integrin a5b1 and Fn1 regulate the remodeling of the plexus endothelium
737 in the 4th pharyngeal arch into the PAA. Isl1 lineages are marked in green. NC-derived
738 cells are in blue. **B.** The expression of integrin a5 in the mesoderm regulates the
739 differentiation of NC-derived cells into VSMCs. The deletion of integrin α5 in Mesp1
740 lineage, which includes the SHF, leads to defective NC-to-VSMC differentiation and
741 results in the regression of the 4th PAAs leading to IAA-B and RERSA (Liang, et al., *Dev*
742 *Biol* 2014). **C.** Fn1 becomes upregulated in NC-derived cells adjacent to the 4th PAA
743 ECs between E10.5 and E11.5 The expression of integrin α5β1 and Fn1 in the NC-
744 derived cells is required for NC-to-VSMC differentiation and the stability of the 4th PAA
745 (Wang et al, 2016). The deletion of either α5 or Fn1 in the NC (and the surface
746 ectoderm) leads to IAA-B and RERSA but does not impair PAA formation.

747

Supplemental Figure 1. Delayed formation of the 4th PAAs in mutants lacking integrin α5 or Fn1 in the Isl1 lineages. A – B. Quantification of total endothelial cell numbers in the 4th arches of controls and mutants show similar phenotypes among integrin $\alpha5^{flox/-}$; Isl1$^{Cre/+}$ and Fn1$^{flox/-}$; Isl1$^{Cre/+}$ embryos. Note the recovery of endothelial cell numbers at 36 – 40-somite stage. **C.** Combined data comparing endothelial populations of controls and integrin $\alpha5^{flox/-}$; Isl1$^{Cre/+}$ and Fn1$^{flox/-}$; Isl1$^{Cre/+}$ mutant embryos at 33 – 34-somite stages. **D.** The proportion of pharyngeal ECs in the plexus is increased in the mutants relative to controls. **E.** The proportion of endothelial cells in the PAA is decreased in the mutants relative to controls. Note, 7 of 16 mutants did not have PAAs (0% endothelial cells in the 4th PAA).

Supplemental Figure 2. The prevalence of cell death, as assayed by the presence of cleaved caspase 3 or TUNEL signals, was similar in controls and mutants. A, C. Controls. **B, D.** Mutants. All scale bars are 100 μm.

Supplemental Figure 3. **The differentiation of SHF-derived cells into endothelial cells is not affected by the deletion of integrin α5 in the Isl1 lineages.** Whole-mount staining, confocal imaging and 3D reconstruction through the pharyngeal regions of control (**A, C**) and mutant (**B, D**) embryos. **A – B.** Sagittal optical sections through E9.5 embryos: The majority of VEGFR2^{+} cells express GFP and ERG in the 3rd PAA and in a more posterior mesenchyme (arrows) in controls and mutants. **C – D.** E10.5 embryos. 3D reconstruction through the pharyngeal region. Open chevrons mark the 4th PAAs.

Note the presence of a very thin PAA in the mutant (**D-D1**). All VERGFR2^{+} cells are Pecam1^{+} in control and in the mutant with defective 4th PAA. Scale bars are 50 μm.

Supplemental Figure 4. Quantification of SHF-derived cells in pharyngeal mesenchyme and splanchnic mesoderm. E9.5 Isl1$^{Cre/+}$; Rosa$^{nTnG/+}$ embryos were stained with anti-GFP antibodies, cleared in BABB, and imaged through the entire pharyngeal region using 25x silicone oil objective N.A. 1.05 and Nikon confocal microscope. 3D reconstruction and surfacing were done using IMARIS. **A.** Pharyngeal mesenchyme in the 1st and 2nd pharyngeal arches was surfaced. Dashed line marks the plane of transverse optical section shown in **A1**. GFP^{+} cells within the pharyngeal mesenchyme (yellow) were quantified using the spot function in IMARIS in the entire volume marked by the yellow surfaces in **A. B –B4**. Splanchnic mesoderm within the dorsal pericardial wall was surfaced in pink, and pharyngeal mesenchyme was surfaced in yellow. **B.** Ventral view. **B1.** Right-side view. Dashed line indicates the plane of section shown in **B3. B2.** A slanted, sagittal/coronal view to visualize both the splanchnic mesoderm and pharyngeal mesenchyme. **B3**. GFP^{+} cells in the splanchnic mesoderm (pink) and in the posterior pharyngeal mesenchyme (yellow) were quantified using the spot function in IMARIS throughout the entire volume shown in **B**.

Supplemental Figure 5. **Step-wise changes in the configuration of the 4th arch endothelium on the 10th day of mouse embryonic development.** Control embryos were stained using antibody to Pecam1. Endothelial cells in the 4th pharyngeal arch were surface-rendered yellow using IMARIS. First row, 30-somite stage. Endothelium in

the 4th arch is in the form of a plexus of small blood vessels. Second row 33-somite embryo. A small PAA is seen forming. Red starts mark spaces amidst the interconnected plexus vessels and the small PAA. Third row, 33-somite stage. A large PAA is seen with connecting plexus vessels. Spaces (marked by the red stars) are still seen. Fourth row – 36 – 40 – somite stage. A large PAA is present in the 4th arch by the evening of the 10th day. DA – dorsal aorta. PAAs are numbers. All scale bars are 50 μm.

Supplemental Figure 6. The expression of integrin α5β1 in the Isl1 lineages regulates the differentiation of neural crest-derived cells into VSCMs at E11.5 Activation of Notch in the pharyngeal arch mesenchyme is not altered in the mutants. Coronal section through the pharyngeal regions of Control (**A**) and Mutant (**B**) embryos were stained to detect green fluorescent protein (GFP, green) marks the Isl1 lineages; Notch intracellular domain (NICD, orange) is used as the readout of active Notch signaling; and a smooth muscle actin (αSMA, blue) marks smooth muscle cells. PAAs are numbered. The magnification is the same in all panels.

Supplemental Figure 7. PAA formation is not affected when integrin α5 is ablated using Sox17$^{2A\text{-}iCre}$ knock-in strain. Whole-mount pictures were taken following India Ink injections into the hearts of controls and mutants isolated at E10.5. Magnification is the same in all panels.

References

1. Stoller JZ and Epstein JA. Cardiac neural crest. *Semin Cell Dev Biol*. 2005;16:704-15.

2. Schreiber C, Mazzitelli D, Haehnel JC, Lorenz HP and Meisner H. The interrupted aortic arch: an overview after 20 years of surgical treatment. *Eur J Cardiothorac Surg*. 1997;12:466-9; discussion 469-70.

3. Kellenberger CJ. Aortic arch malformations. *Pediatr Radiol*. 2010;40:876-84.

4. Psillas G, Kekes G, Constantinidis J, Triaridis S and Vital V. Subclavian steal syndrome: neurotological manifestations. *Acta Otorhinolaryngol Ital*. 2007;27:33-7.

5. Kirby ML. *Cardiac Development*. New York: Oxford University Press; 2007.

6. Moon A. Mouse models of congenital cardiovascular disease. *Curr Top Dev Biol*. 2008;84:171-248.

7. Nagelberg D, Wang J, Su R, Torres-Vazquez J, Targoff KL, Poss KD and Knaut H. Origin, Specification, and Plasticity of the Great Vessels of the Heart. *Curr Biol*. 2015;25:2099-110.

8. Paffett-Lugassy N, Singh R, Nevis KR, Guner-Ataman B, O'Loughlin E, Jahangiri L, Harvey RP, Burns CG and Burns CE. Heart field origin of great vessel precursors relies on nkx2.5-mediated vasculogenesis. *Nat Cell Biol*. 2013;15:1362-9.

9. Wang X, Chen D, Chen K, Jubran A, Ramirez A and Astrof S. Endothelium in the pharyngeal arches 3, 4 and 6 is derived from the second heart field. *Dev Biol*. 2017;421:108-117.

10. Li P, Pashmforoush M and Sucov HM. Mesodermal retinoic acid signaling regulates endothelial cell coalescence in caudal pharyngeal arch artery vasculogenesis. *Dev Biol*. 2012;361:116-24.

11. Bremer JL. The development of the aorta and aortic arches in rabbits. *American Journal of Anatomy*. 1912;13:111-128.

12. DeRuiter MC, Poelmann RE, Mentink MM, Vaniperen L and Gittenberger-De Groot AC. Early formation of the vascular system in quail embryos. *Anat Rec*. 1993;235:261-74.

13. Abrial M, Paffett-Lugassy N, Jeffrey S, Jordan D, O'Loughlin E, Frederick CJ, 3rd, Burns CG and Burns CE. TGF-beta Signaling Is Necessary and Sufficient for Pharyngeal Arch Artery Angioblast Formation. *Cell Rep*. 2017;20:973-983.

14. Guner-Ataman B, Paffett-Lugassy N, Adams MS, Nevis KR, Jahangiri L, Obregon P, Kikuchi K, Poss KD, Burns CE and Burns CG. Zebrafish second heart field development relies on progenitor specification in anterior lateral plate mesoderm and nkx2.5 function. *Development*. 2013;140:1353-63.

15. Guner-Ataman B, Gonzalez-Rosa JM, Shah HN, Butty VL, Jeffrey S, Abrial M, Boyer LA, Burns CG and Burns CE. Failed Progenitor Specification Underlies the Cardiopharyngeal Phenotypes in a Zebrafish Model of 22q11.2 Deletion Syndrome. *Cell Rep*. 2018;24:1342-1354 e5.

16. Holowiecki A, Linstrum K, Ravisankar P, Chetal K, Salomonis N and Waxman JS. Pbx4 limits heart size and fosters arch artery formation through partitioning second heart field progenitors and restricting proliferation. *Development*. 2020.

17. Gittenberger-de Groot AC, DeRuiter MC, Bergwerff M and Poelmann RE. Smooth muscle cell origin and its relation to heterogeneity in development and disease. *Arterioscler Thromb Vasc Biol*. 1999;19:1589-94.

18. Bockman DE, Redmond ME, Waldo K, Davis H and Kirby ML. Effect of neural crest ablation on development of the heart and arch arteries in the chick. *The American journal of anatomy*. 1987;180:332-41.

19. Hutson MR and Kirby ML. Model systems for the study of heart development and disease. Cardiac neural crest and conotruncal malformations. *Semin Cell Dev Biol*. 2007;18:101-10.

20. Hutson MR, Sackey FN, Lunney K and Kirby ML. Blocking hedgehog signaling after ablation of the dorsal neural tube allows regeneration of the cardiac neural crest and rescue of outflow tract septation. *Dev Biol*. 2009;335:367-73.

21. Rosenquist TH, Kirby ML and van Mierop LH. Solitary aortic arch artery. A result of surgical ablation of cardiac neural crest and nodose placode in the avian embryo. *Circulation*. 1989;80:1469-75.

22. Keyte A and Hutson MR. The neural crest in cardiac congenital anomalies. *Differentiation; research in biological diversity*. 2012;84:25-40.

23. Coles EG, Gammill LS, Miner JH and Bronner-Fraser M. Abnormalities in neural crest cell migration in laminin alpha5 mutant mice. *Dev Biol*. 2006;289:218-28.

876 24. Cooley MA, Kern CB, Fresco VM, Wessels A, Thompson RP, McQuinn TC, Twal
877 WO, Mjaatvedt CH, Drake CJ and Argraves WS. Fibulin-1 is required for
878 morphogenesis of neural crest-derived structures. *Dev Biol*. 2008;319:336-45.

879 25. Rydeen AB and Waxman JS. Cyp26 Enzymes Facilitate Second Heart Field
880 Progenitor Addition and Maintenance of Ventricular Integrity. *PLoS Biol*.
881 2016;14:e2000504.

882 26. Wickstrom SA, Radovanac K and Fassler R. Genetic analyses of integrin
883 signaling. *Cold Spring Harb Perspect Biol*. 2011;3.

884 27. Astrof S. Interactions between neural crest-derived cells and extracellular
885 microenvironment during cardiovascular development. In: D. W. Desimone and R. P.
886 Mecham, eds. *Extracellular Matrix in Development* Berlin: Springer Verlag; 2013: 105-
887 131.

888 28. Mittal A, Pulina M, Hou SY and Astrof S. Fibronectin and integrin alpha 5 play
889 essential roles in the development of the cardiac neural crest. *Mech Dev*. 2010;127:472-
890 84.

891 29. Chen D, Wang X, Liang D, Gordon J, Mittal A, Manley N, Degenhardt K and
892 Astrof S. Fibronectin signals through integrin alpha5beta1 to regulate cardiovascular
893 development in a cell type-specific manner. *Dev Biol*. 2015;407:195-210.

894 30. Wang X and Astrof S. Isolation of Mouse Cardiac Neural Crest Cells and Their
895 Differentiation into Smooth Muscle Cells. *Bio Protoc*. 2017;7.

896 31. Wang X and Astrof S. Neural crest cell-autonomous roles of fibronectin in
897 cardiovascular development. *Development*. 2016;143:88-100.

898 32. Humphries JD, Byron A and Humphries MJ. Integrin ligands at a glance. *J Cell
899 Sci*. 2006;119:3901-3.

900 33. Hynes RO and Naba A. Overview of the matrisome--an inventory of extracellular
901 matrix constituents and functions. *Cold Spring Harbor perspectives in biology*.
902 2012;4:a004903.

903 34. Pulina M, Liang D and Astrof S. Shape and position of the node and notochord
904 along the bilateral plane of symmetry are regulated by cell-extracellular matrix
905 interactions. *Biology open*. 2014;3:583-90.

35. George EL, Baldwin HS and Hynes RO. Fibronectins are essential for heart and blood vessel morphogenesis but are dispensable for initial specification of precursor cells. *Blood*. 1997;90:3073-81.

36. George EL, Georges-Labouesse EN, Patel-King RS, Rayburn H and Hynes RO. Defects in mesoderm, neural tube and vascular development in mouse embryos lacking fibronectin. *Development*. 1993;119:1079-91.

37. Georges-Labouesse EN, George EL, Rayburn H and Hynes RO. Mesodermal development in mouse embryos mutant for fibronectin. *Dev Dyn*. 1996;207:145-56.

38. Pulina MV, Hou SY, Mittal A, Julich D, Whittaker CA, Holley SA, Hynes RO and Astrof S. Essential roles of fibronectin in the development of the left-right embryonic body plan. *Dev Biol*. 2011;354:208-20.

39. Yang JT, Bader BL, Kreidberg JA, Ullman-Cullere M, Trevithick JE and Hynes RO. Overlapping and independent functions of fibronectin receptor integrins in early mesodermal development. *Dev Biol*. 1999;215:264-77.

40. Yang JT, Rayburn H and Hynes RO. Embryonic mesodermal defects in alpha 5 integrin-deficient mice. *Development*. 1993;119:1093-105.

41. Mittal A, Pulina M, Hou S and Astrof S. Fibronectin and integrin alpha 5 play requisite roles in cardiac morphogenesis. *Dev Biol*. 2013;381:73-82.

42. Sun Y, Liang X, Najafi N, Cass M, Lin L, Cai CL, Chen J and Evans SM. Islet 1 is expressed in distinct cardiovascular lineages, including pacemaker and coronary vascular cells. *Dev Biol*. 2007;304:286-96.

43. Devine WP, Wythe JD, George M, Koshiba-Takeuchi K and Bruneau BG. Early patterning and specification of cardiac progenitors in gastrulating mesoderm. *eLife*. 2014;3.

44. Ramirez A and Astrof S. Visualization and Analysis of Pharyngeal Arch Arteries using Whole-mount Immunohistochemistry and 3D Reconstruction. *J Vis Exp*. 2020;157:e60797.

45. Fish JE, Cantu Gutierrez M, Dang LT, Khyzha N, Chen Z, Veitch S, Cheng HS, Khor M, Antounians L, Njock MS, Boudreau E, Herman AM, Rhyner AM, Ruiz OE, Eisenhoffer GT, Medina-Rivera A, Wilson MD and Wythe JD. Dynamic regulation of VEGF-inducible genes by an ERK/ERG/p300 transcriptional network. *Development*. 2017;144:2428-2444.

938 46. Jia G, Preussner J, Chen X, Guenther S, Yuan X, Yekelchyk M, Kuenne C,
939 Looso M, Zhou Y, Teichmann S and Braun T. Single cell RNA-seq and ATAC-seq
940 analysis of cardiac progenitor cell transition states and lineage settlement. *Nat*
941 *Commun*. 2018;9:4877.

942 47. Verzi MP, McCulley DJ, De Val S, Dodou E and Black BL. The right ventricle,
943 outflow tract, and ventricular septum comprise a restricted expression domain within the
944 secondary/anterior heart field. *Dev Biol*. 2005;287:134-45.

945 48. Dodou E, Verzi MP, Anderson JP, Xu SM and Black BL. Mef2c is a direct
946 transcriptional target of ISL1 and GATA factors in the anterior heart field during mouse
947 embryonic development. *Development*. 2004;131:3931-42.

948 49. Papangeli I and Scambler PJ. Tbx1 genetically interacts with the transforming
949 growth factor-beta/bone morphogenetic protein inhibitor Smad7 during great vessel
950 remodeling. *Circ Res*. 2013;112:90-102.

951 50. Lindsay EA and Baldini A. Recovery from arterial growth delay reduces
952 penetrance of cardiovascular defects in mice deleted for the DiGeorge syndrome
953 region. *Human molecular genetics*. 2001;10:997-1002.

954 51. Waldo KL, Kumiski D and Kirby ML. Cardiac neural crest is essential for the
955 persistence rather than the formation of an arch artery. *Dev Dyn*. 1996;205:281-92.

956 52. High FA, Zhang M, Proweller A, Tu L, Parmacek MS, Pear WS and Epstein JA.
957 An essential role for Notch in neural crest during cardiovascular development and
958 smooth muscle differentiation. *J Clin Invest*. 2007;117:353-63.

959 53. High FA, Jain R, Stoller JZ, Antonucci NB, Lu MM, Loomes KM, Kaestner KH,
960 Pear WS and Epstein JA. Murine Jagged1/Notch signaling in the second heart field
961 orchestrates Fgf8 expression and tissue-tissue interactions during outflow tract
962 development. *J Clin Invest*. 2009;119:1986-96.

963 54. High FA, Lu MM, Pear WS, Loomes KM, Kaestner KH and Epstein JA.
964 Endothelial expression of the Notch ligand Jagged1 is required for vascular smooth
965 muscle development. *Proceedings of the National Academy of Sciences %R*
966 *101073/pnas0709663105*. 2008;105:1955-1959.

967 55. Manderfield LJ, Aghajanian H, Engleka KA, Lim LY, Lui F, Jain R, Li L, Olson EN
968 and Epstein JA. Hippo signaling is required for Notch-dependent smooth muscle
969 differentiation of neural crest. *Development*. 2015.

970 56. Manderfield LJ, High FA, Engleka KA, Liu F, Li L, Rentschler S and Epstein JA.
971 Notch activation of Jagged1 contributes to the assembly of the arterial wall. *Circulation*.
972 2012;125:314-23.

973 57. Hellstrom M, Gerhardt H, Kalen M, Li X, Eriksson U, Wolburg H and Betsholtz C.
974 Lack of pericytes leads to endothelial hyperplasia and abnormal vascular
975 morphogenesis. *J Cell Biol*. 2001;153:543-53.

976 58. Jiang X, Rowitch DH, Soriano P, McMahon AP and Sucov HM. Fate of the
977 mammalian cardiac neural crest. *Development*. 2000;127:1607-1616.

978 59. Liang D, Wang X, Mittal A, Dhiman S, Hou SY, Degenhardt K and Astrof S.
979 Mesodermal expression of integrin alpha5beta1 regulates neural crest development and
980 cardiovascular morphogenesis. *Dev Biol*. 2014;395:232–244.

981 60. Engleka KA, Manderfield LJ, Brust RD, Li L, Cohen A, Dymecki SM and Epstein
982 JA. Islet1 derivatives in the heart are of both neural crest and second heart field origin.
983 *Circ Res*. 2012;110:922-6.

984 61. van der Flier A, Badu-Nkansah K, Whittaker CA, Crowley D, Bronson RT, Lacy-
985 Hulbert A and Hynes RO. Endothelial alpha5 and alphav integrins cooperate in
986 remodeling of the vasculature during development. *Development*. 2010;137:2439-49.

987 62. Engert S, Liao WP, Burtscher I and Lickert H. Sox17-2A-iCre: a knock-in mouse
988 line expressing Cre recombinase in endoderm and vascular endothelial cells. *Genesis*.
989 2009;47:603-10.

990 63. Calmont A, Ivins S, Van Bueren KL, Papangeli I, Kyriakopoulou V, Andrews WD,
991 Martin JF, Moon AM, Illingworth EA, Basson MA and Scambler PJ. Tbx1 controls
992 cardiac neural crest cell migration during arch artery development by regulating Gbx2
993 expression in the pharyngeal ectoderm. *Development*. 2009;136:3173-83.

994 64. Gitler AD, Lu MM and Epstein JA. PlexinD1 and semaphorin signaling are
995 required in endothelial cells for cardiovascular development. *Dev Cell*. 2004;7:107-16.

996 65. Merscher S, Funke B, Epstein JA, Heyer J, Puech A, Lu MM, Xavier RJ, Demay
997 MB, Russell RG, Factor S, Tokooya K, Jore BS, Lopez M, Pandita RK, Lia M, Carrion
998 D, Xu H, Schorle H, Kobler JB, Scambler P, Wynshaw-Boris A, Skoultchi AI, Morrow BE
999 and Kucherlapati R. TBX1 is responsible for cardiovascular defects in velo-cardio-
1000 facial/DiGeorge syndrome. *Cell*. 2001;104:619-29.

1001 66. Phillips HM, Stothard CA, Shaikh Qureshi WM, Kousa AI, Briones-Leon JA,
1002 Khasawneh RR, O'Loughlin C, Sanders R, Mazzotta S, Dodds R, Seidel K, Bates T,

1003 Nakatomi M, Cockell SJ, Schneider JE, Mohun TJ, Maehr R, Kist R, Peters H and
1004 Bamforth SD. Pax9 is required for cardiovascular development and interacts with Tbx1
1005 in the pharyngeal endoderm to control 4th pharyngeal arch artery morphogenesis.
1006 *Development*. 2019;146.

1007 67. Macatee TL, Hammond BP, Arenkiel BR, Francis L, Frank DU and Moon AM.
1008 Ablation of specific expression domains reveals discrete functions of ectoderm- and
1009 endoderm-derived FGF8 during cardiovascular and pharyngeal development.
1010 *Development*. 2003;130:6361-74.

1011 68. Cai CL, Liang X, Shi Y, Chu PH, Pfaff SL, Chen J and Evans S. Isl1 identifies a
1012 cardiac progenitor population that proliferates prior to differentiation and contributes a
1013 majority of cells to the heart. *Dev Cell*. 2003;5:877-89.

1014 69. Baldini A, Fulcoli FG and Illingworth E. Tbx1: Transcriptional and Developmental
1015 Functions. *Current topics in developmental biology*. 2017;122:223-243.

1016 70. Graham A, Okabe M and Quinlan R. The role of the endoderm in the
1017 development and evolution of the pharyngeal arches. *J Anat*. 2005;207:479-87.

1018 71. Alfano D, Altomonte A, Cortes C, Bilio M, Kelly RG and Baldini A. Tbx1 regulates
1019 extracellular matrix-cell interactions in the second heart field. *Human molecular*
1020 *genetics*. 2019;28:2295-2308.

1021 72. Francou A, Saint-Michel E, Mesbah K and Kelly RG. TBX1 regulates epithelial
1022 polarity and dynamic basal filopodia in the second heart field. *Development*.
1023 2014;141:4320-31.

1024 73. van Bueren KL, Papangeli I, Rochais F, Pearce K, Roberts C, Calmont A,
1025 Szumska D, Kelly RG, Bhattacharya S and Scambler PJ. Hes1 expression is reduced in
1026 Tbx1 null cells and is required for the development of structures affected in 22q11
1027 deletion syndrome. *Dev Biol*. 2010;340:369-80.

1028 74. Aghajanian H, Choi C, Ho VC, Gupta M, Singh MK and Epstein JA. Semaphorin
1029 3d and semaphorin 3e direct endothelial motility through distinct molecular signaling
1030 pathways. *J Biol Chem*. 2014;289:17971-9.

1031 75. Cohen ED, Wang Z, Lepore JJ, Lu MM, Taketo MM, Epstein DJ and Morrisey
1032 EE. Wnt/beta-catenin signaling promotes expansion of Isl-1-positive cardiac progenitor
1033 cells through regulation of FGF signaling. *J Clin Invest*. 2007;117:1794-804.

1034 76. Degenhardt K, Singh MK, Aghajanian H, Massera D, Wang Q, Li J, Li L, Choi C,
1035 Yzaguirre AD, Francey LJ, Gallant E, Krantz ID, Gruber PJ and Epstein JA. Semaphorin

3d signaling defects are associated with anomalous pulmonary venous connections. *Nat Med*. 2013;19:760-5.

77. Frank DU, Fotheringham LK, Brewer JA, Muglia LJ, Tristani-Firouzi M, Capecchi MR and Moon AM. An Fgf8 mouse mutant phenocopies human 22q11 deletion syndrome. *Development*. 2002;129:4591-603.

78. Park EJ, Ogden LA, Talbot A, Evans S, Cai CL, Black BL, Frank DU and Moon AM. Required, tissue-specific roles for Fgf8 in outflow tract formation and remodeling. *Development*. 2006;133:2419-33.

79. Park EJ, Watanabe Y, Smyth G, Miyagawa-Tomita S, Meyers E, Klingensmith J, Camenisch T, Buckingham M and Moon AM. An FGF autocrine loop initiated in second heart field mesoderm regulates morphogenesis at the arterial pole of the heart. *Development*. 2008;135:3599-610.

80. Watanabe Y, Miyagawa-Tomita S, Vincent SD, Kelly RG, Moon AM and Buckingham ME. Role of mesodermal FGF8 and FGF10 overlaps in the development of the arterial pole of the heart and pharyngeal arch arteries. *Circ Res*. 2010;106:495-503.

81. Stalmans I, Lambrechts D, De Smet F, Jansen S, Wang J, Maity S, Kneer P, von der Ohe M, Swillen A, Maes C, Gewillig M, Molin DG, Hellings P, Boetel T, Haardt M, Compernolle V, Dewerchin M, Plaisance S, Vlietinck R, Emanuel B, Gittenberger-de Groot AC, Scambler P, Morrow B, Driscol DA, Moons L, Esguerra CV, Carmeliet G, Behn-Krappa A, Devriendt K, Collen D, Conway SJ and Carmeliet P. VEGF: a modifier of the del22q11 (DiGeorge) syndrome? *Nat Med*. 2003;9:173-82.

82. Oh J, Richardson JA and Olson EN. Requirement of myocardin-related transcription factor-B for remodeling of branchial arch arteries and smooth muscle differentiation. *Proc Natl Acad Sci U S A*. 2005;102:15122-7.

83. Hellstrom M, Kalen M, Lindahl P, Abramsson A and Betsholtz C. Role of PDGF-B and PDGFR-beta in recruitment of vascular smooth muscle cells and pericytes during embryonic blood vessel formation in the mouse. *Development*. 1999;126:3047-55.

84. Scambler PJ. The 22q11 deletion syndromes. *Human molecular genetics*. 2000;9:2421-6.

85. Momma K. Cardiovascular anomalies associated with chromosome 22q11.2 deletion syndrome. *Am J Cardiol*. 2010;105:1617-24.

86. Lindsay EA, Vitelli F, Su H, Morishima M, Huynh T, Pramparo T, Jurecic V, Ogunrinu G, Sutherland HF, Scambler PJ, Bradley A and Baldini A. Tbx1

haploinsufficieny in the DiGeorge syndrome region causes aortic arch defects in mice. *Nature*. 2001;410:97-101.

87. Jerome LA and Papaioannou VE. DiGeorge syndrome phenotype in mice mutant for the T-box gene, Tbx1. *Nat Genet*. 2001;27:286-91.

FIGURE 1

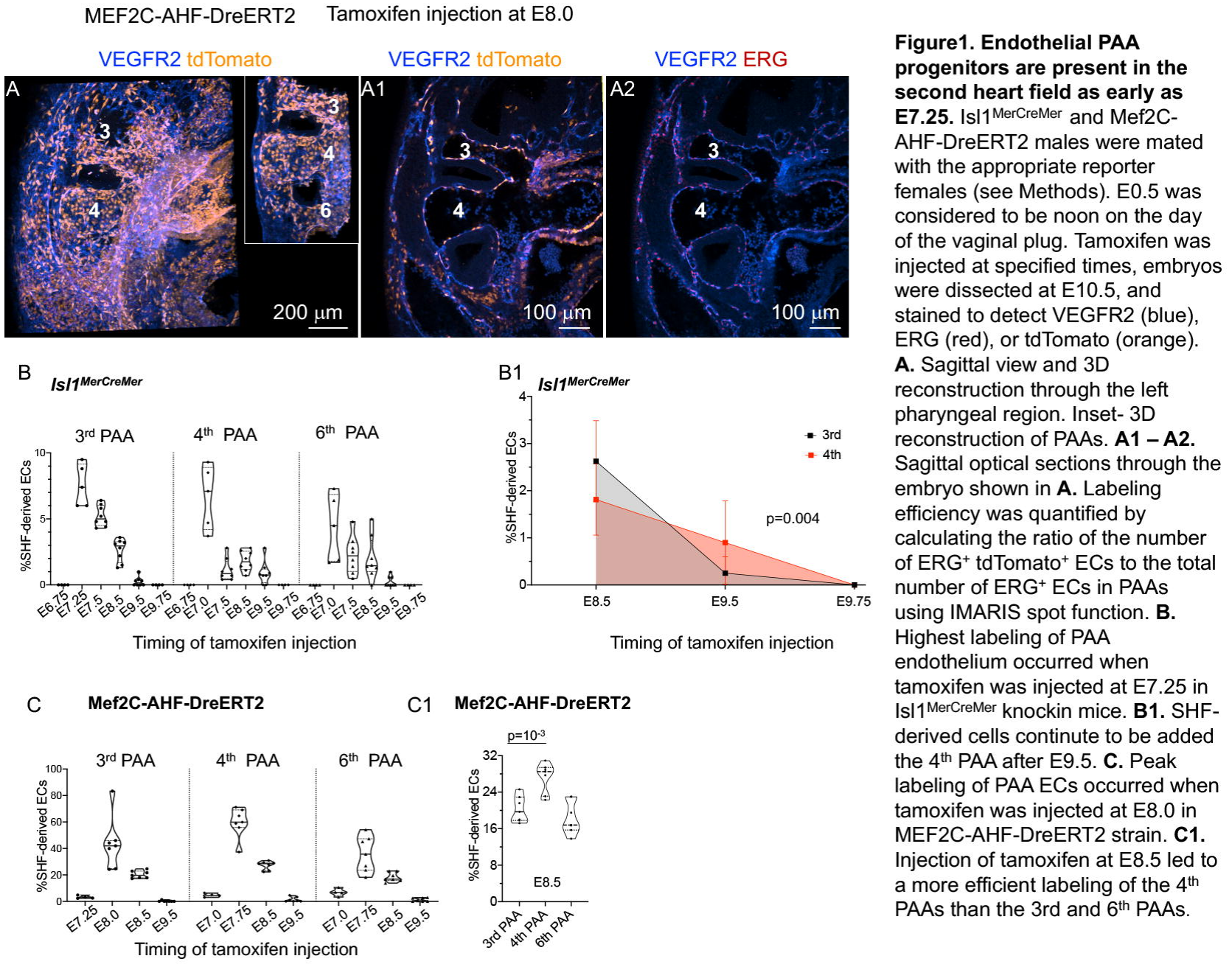

Figure1. Endothelial PAA progenitors are present in the second heart field as early as E7.25. Isl1^{MerCreMer} and Mef2C-AHF-DreERT2 males were mated with the appropriate reporter females (see Methods). E0.5 was considered to be noon on the day of the vaginal plug. Tamoxifen was injected at specified times, embryos were dissected at E10.5, and stained to detect VEGFR2 (blue), ERG (red), or tdTomato (orange). **A.** Sagittal view and 3D reconstruction through the left pharyngeal region. Inset- 3D reconstruction of PAAs. **A1 – A2.** Sagittal optical sections through the embryo shown in **A.** Labeling efficiency was quantified by calculating the ratio of the number of ERG$^+$ tdTomato$^+$ ECs to the total number of ERG$^+$ ECs in PAAs using IMARIS spot function. **B.** Highest labeling of PAA endothelium occurred when tamoxifen was injected at E7.25 in Isl1^{MerCreMer} knockin mice. **B1.** SHF-derived cells continute to be added the 4th PAA after E9.5. **C.** Peak labeling of PAA ECs occurred when tamoxifen was injected at E8.0 in MEF2C-AHF-DreERT2 strain. **C1.** Injection of tamoxifen at E8.5 led to a more efficient labeling of the 4th PAAs than the 3rd and 6th PAAs.

FIGURE 2

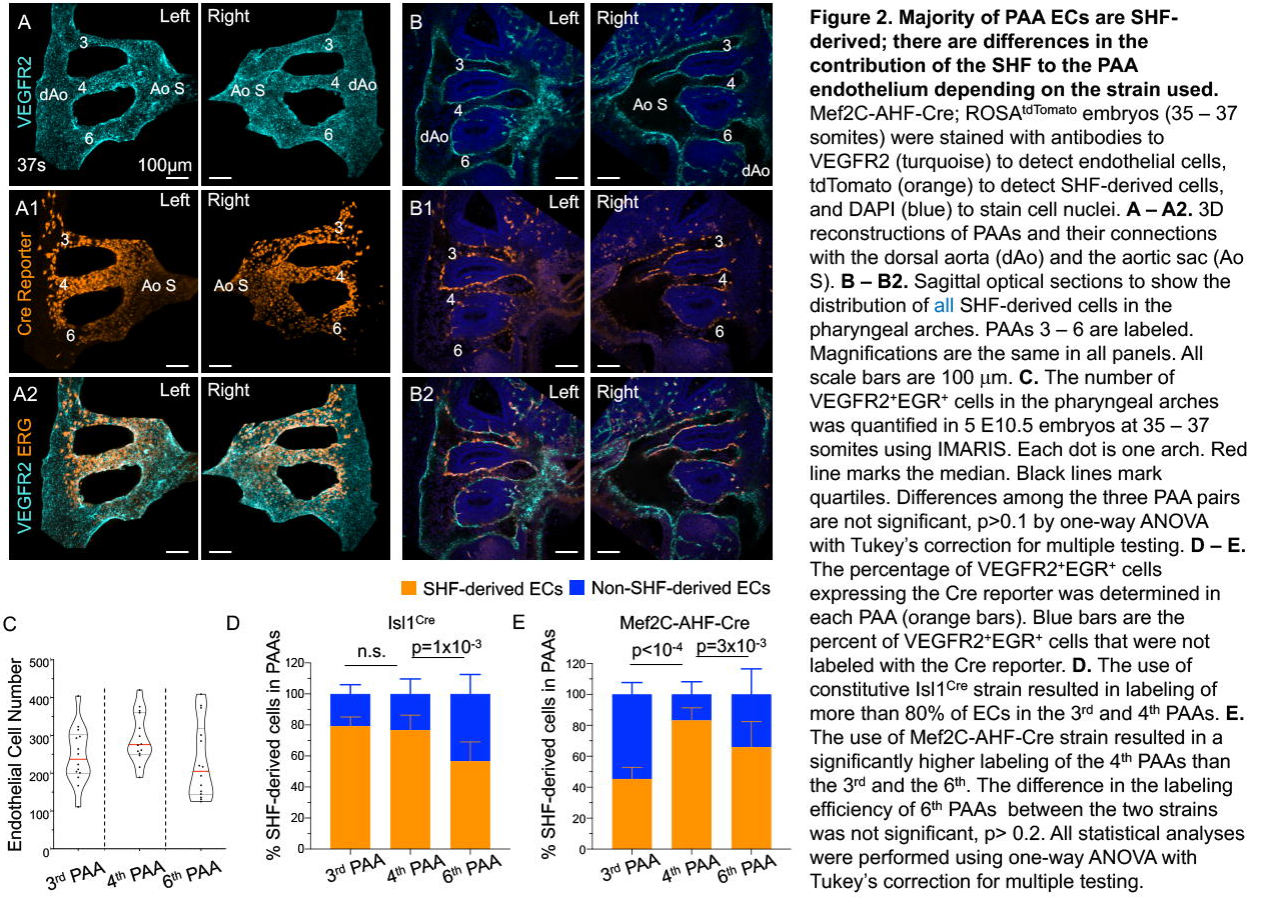

Figure 2. Majority of PAA ECs are SHF-derived; there are differences in the contribution of the SHF to the PAA endothelium depending on the strain used. Mef2C-AHF-Cre; ROSA^{tdTomato} embryos (35 – 37 somites) were stained with antibodies to VEGFR2 (turquoise) to detect endothelial cells, tdTomato (orange) to detect SHF-derived cells, and DAPI (blue) to stain cell nuclei. **A – A2.** 3D reconstructions of PAAs and their connections with the dorsal aorta (dAo) and the aortic sac (Ao S). **B – B2.** Sagittal optical sections to show the distribution of all SHF-derived cells in the pharyngeal arches. PAAs 3 – 6 are labeled. Magnifications are the same in all panels. All scale bars are 100 μm. **C.** The number of VEGFR2^{+}EGR^{+} cells in the pharyngeal arches was quantified in 5 E10.5 embryos at 35 – 37 somites using IMARIS. Each dot is one arch. Red line marks the median. Black lines mark quartiles. Differences among the three PAA pairs are not significant, p>0.1 by one-way ANOVA with Tukey's correction for multiple testing. **D – E.** The percentage of VEGFR2^{+}EGR^{+} cells expressing the Cre reporter was determined in each PAA (orange bars). Blue bars are the percent of VEGFR2^{+}EGR^{+} cells that were not labeled with the Cre reporter. **D.** The use of constitutive Isl1^{Cre} strain resulted in labeling of more than 80% of ECs in the 3rd and 4th PAAs. **E.** The use of Mef2C-AHF-Cre strain resulted in a significantly higher labeling of the 4th PAAs than the 3rd and the 6th. The difference in the labeling efficiency of 6th PAAs between the two strains was not significant, p> 0.2. All statistical analyses were performed using one-way ANOVA with Tukey's correction for multiple testing.

FIGURE 3

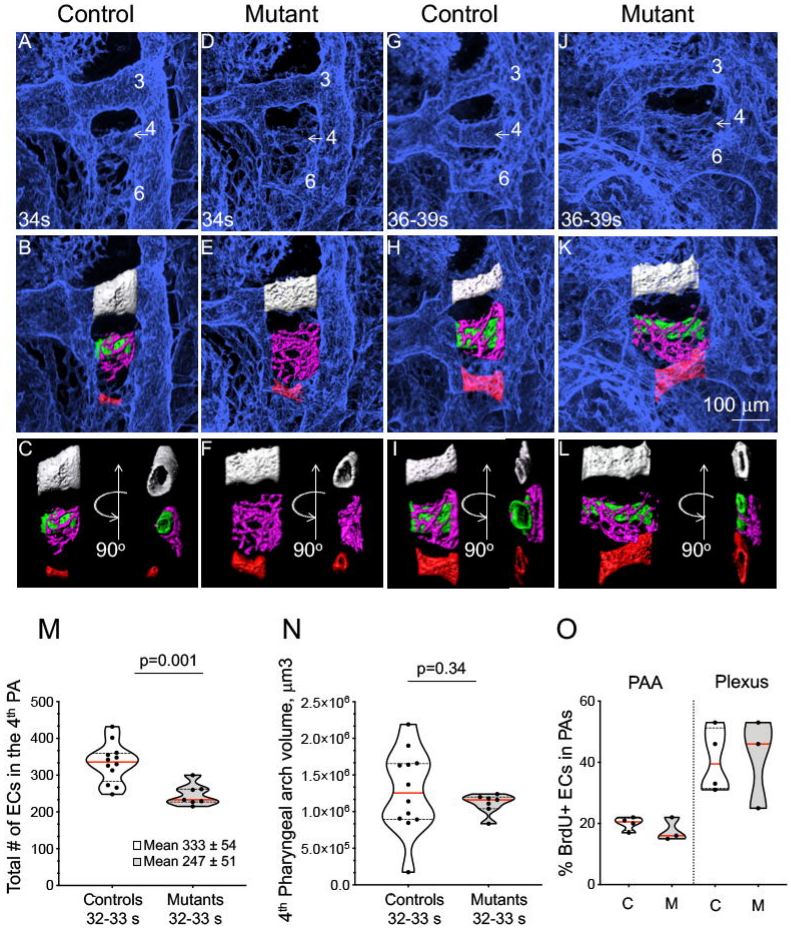

Figure 3. Formation of the 4th PAA is delayed in integrin $\alpha5^{flox/-}$; $Isl1^{Cre}$ mutants. $\alpha5^{flox/+}$; $Isl1^{Cre}$ control and $\alpha5^{flox/-}$; $Isl1^{Cre}$ mutant embryos were dissected at different somite stages at E10.5 and stained to detect Pecam1. PAAs are numbered and somite stages are indicated in the first row. **A, D, G, J.** 3D reconstructions of whole-mount Pecam 1 staining (light blue). **B, E, H, K.** PAA endothelium in the 3rd, 4th and 6th arches shown in the row above was surface-rendered white, green and red, respectively. In addition, the plexus endothelium in the 4th arch was surface-rendered in pink. **C, F, I, L.** Left side and ventral views of surface-rendered PAAs and the plexus. Development of the 4th PAAs was specifically affected in the mutants (**E, F**). Magnification is the same in all panels. Scale bar is 100 μm. **M**. Total number of endothelial cells was quantified as described in Methods. Mutants have EC deficiency in the 4th arch as 32 – 33 somites. **N.** The sizes of the 4th arches are comparable between controls and mutants. **O.** EC proliferation in the PAA and plexus in the 4th arches was similar in controls (C) and mutants (M). In all plots, solid lines mark the median, dashed lines mark the quartiles. Each dot marks one arch. At least 3 mutants and 3 controls were assayed. Statistics were evaluated using 2-tailed, unpaired Student's t test with Welch's correction for unequal standard deviation between samples.

FIGURE 4

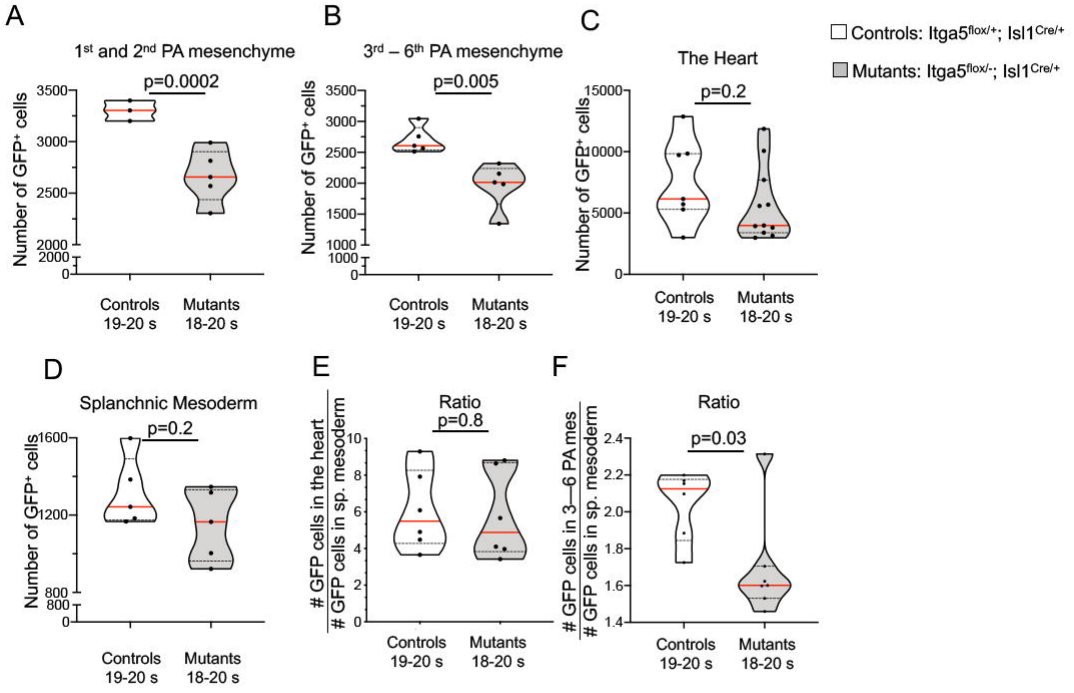

Figure 4. The expression of integrin α5 in the Isl1 lineages is required for the accrual of SHF-derived cells to the pharyngeal mesenchyme. Control and mutant embryos carrying one ROSA^{nTnG} reporter allele were dissected at E9.5 (18 – 20 somite stage) and stained with DAPI and anti-GFP antibodies. Whole embryos were imaged and the number of GFP$^+$ cells (SHF-derivatives) in the arch mesenchyme, splanchnic mesoderm, and in the heart was quantified as described in Sup. Fig. 4. **A.** The total number of SHF cells in the mesenchyme of the 1st and 2nd arches was decreased in the mutants. **B.** The total number of of GFP$^+$ cells in the pharyngeal mesenchyme corresponding with the future arches 3 – 6 was decreased in the mutants. The number of SHF cells in heart (**C**) and the splanchnic mesoderm (**D**) was not affected. **E.** The proportion of GFP$^+$ cells in the heart relative to GFP$^+$ cells in splanchnic mesoderm was not affected in the mutants. **F.** The proportion of GFP$^+$ cells in the posterior pharyngeal mesenchyme relative to the number of GFP$^+$ cells in splanchnic mesoderm was significantly decreased in the mutants. Each dot marks one embryo, red lines mark medians, dotted lines mark quartiles; p values were determined using unpaired, 2-tailed Student's t tests.

FIGURE 5

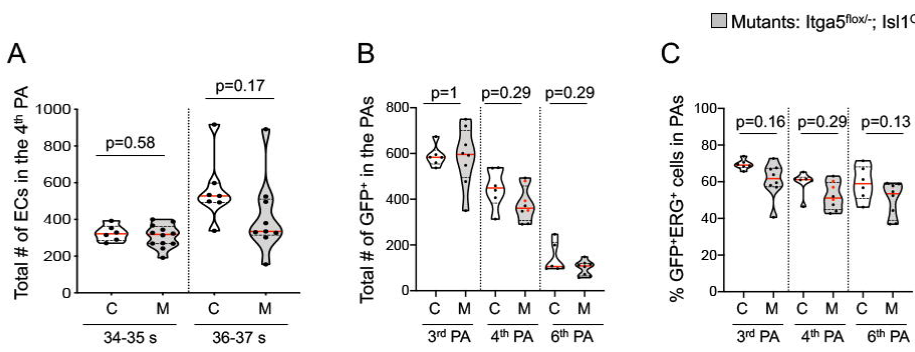

Figure 5. **Recovery of EC numbers in integrin $\alpha5^{flox/-}$; $Isl1^{Cre/+}$ mutants. A.** Total EC number has recovered in integrin $\alpha5^{flox/-}$; $Isl1^{Cre/+}$ mutants by the 34th somite stage. **B.** Total number of SHF-derived mesodermal cells has recovered in the pharyngeal arches in integrin $\alpha5^{flox/-}$; $Isl1^{Cre/+}$ mutants by the 34th somite stage. **C.** The fraction of SHF-derived ECs in pharyngeal arches is comparable among control and mutant embryos. This fraction was calculated by quantifying the number of GFP^+ERG^+ cells and dividing by the total number of ERG^+ cells in the entire pharyngeal arches (e.g. ECs in PAA and plexus were quantified). Statistical significance was evaluated using one-way ANOVA with Tukey's correction for multiple testing.

FIGURE 6

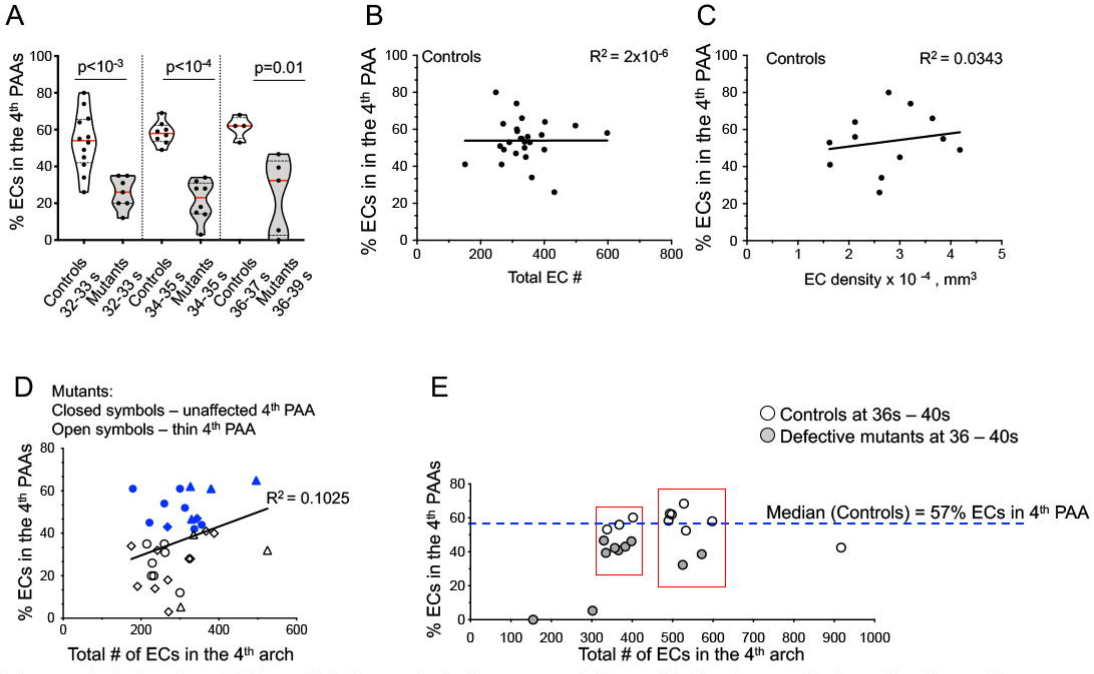

Figure 6. Integrin α5β1 and Fn1 regulate the remodeling of EC plexus during the formation of the 4th pharyngeal arch arteries. A. The proportion of ECs in the 4th PAAs in the mutant is significantly lower than in controls at all stages analyzed at E10.5, including the stages when the EC population in the 4th pharyngeal arch has recovered in the mutants; 2-tailed, unpaired Student's t test. **B – C.** Linear regression analyses indicate the absence of linear correlation between the size of the 4th PAA and EC number (**B**) or density (**C**). PAA size is expressed as the percentage of pharyngeal arch endothelial cells in the 4th PAA in control embryos on the y-axis. **D.** Total EC number (x-axis) from mutants with defective (open symbols) or unaffected 4th PAA (closed symbols) were plotted against the size of the 4th PAAs, y -axis. Regression analysis indicated low correlation between these properties. Circles: 32 – 33 somite embryos, rhombi: 34 – 35 somite embryos, triangles: 36 – 39 somite embryos. **E.** The rearrangement of the endothelial plexus into the 4th PAAs is defective in mutants relative to controls with the same number of endothelial cells in the 4th arch (red boxes). EC – endothelial cell(s). Controls: $\alpha5^{f/+}$; $Isl1^{Cre/+}$ and $Fn1^{f/+}$; $Isl1^{Cre/+}$ embryos; Mutants: $\alpha5^{f/-}$; $Isl1^{Cre/+}$ and $Fn1^{f/-}$; $Isl1^{Cre/+}$ embryos.

FIGURE 7

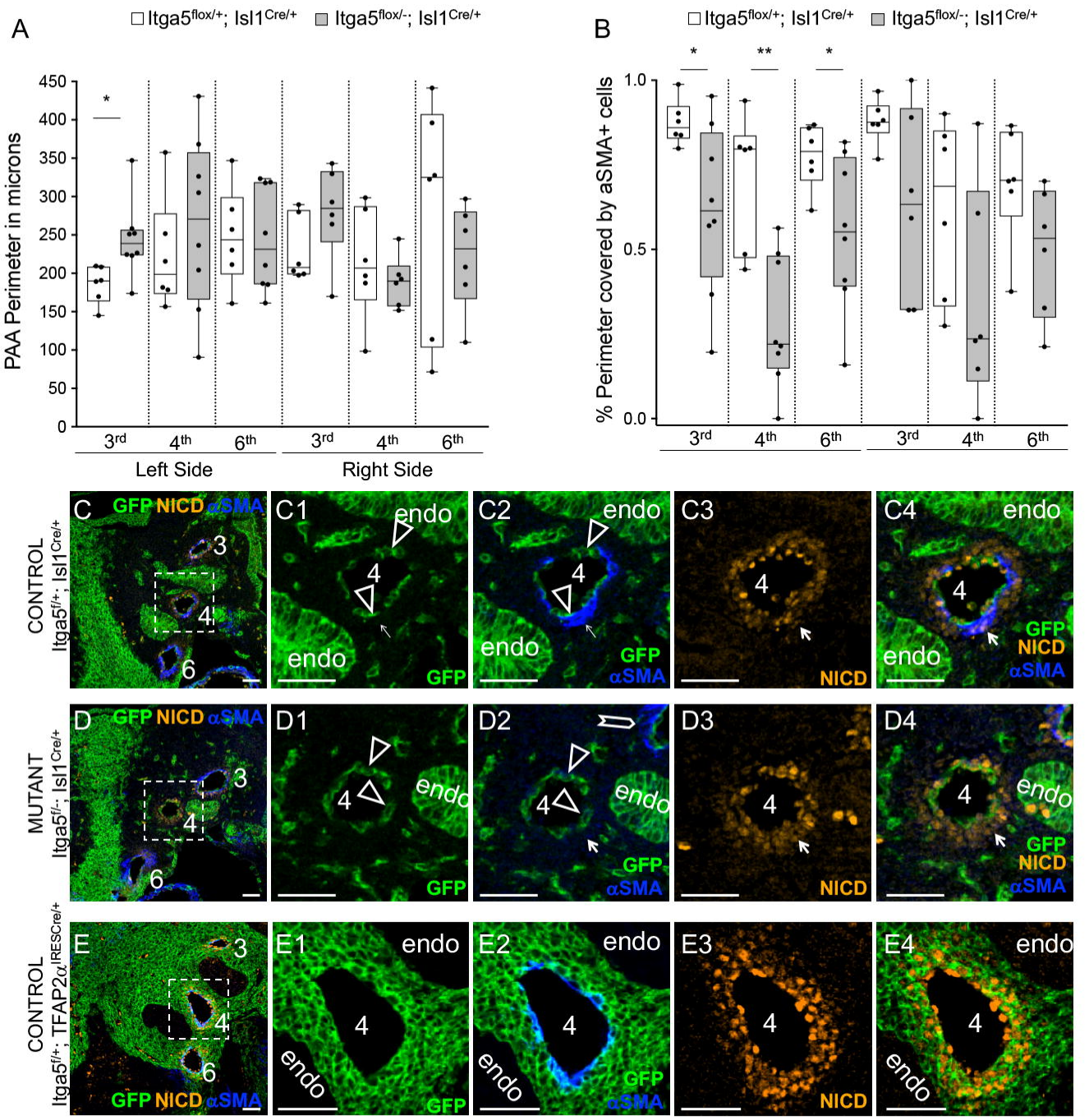

Figure 7. The expression of integrin α5β1 in the Isl1 lineages regulates the differentiation of neural crest-derived cells into VSCMs at E11.5 A. PAA perimeter has recovered in size in the mutants by E11.5. **B.** Smooth muscle coverage of the left 4th and left 6th PAA was deficient in the mutants. **C – D**. Despite defective differentiation of NC cells into VSMCs, the activation of Notch in the pharyngeal arch mesenchyme was not altered in the mutants. PAAs are numbered. PAA ECs at E11.5 are derived from the Isl1^{Cre} lineage (green, arrowheads in **C1, C2** and **D1, D2**). **C2 – D2**. VSMC differentiation assayed by the expression of alpha smooth muscle actin (αSMA, blue) is specifically affected around the 4th PAAs in the mutants (compare regions marked by the arrows in **C2** and **D2**). The activation of Notch assayed by the expression of NICD is not altered in the mutants with defective VSCM differentiation (arrows in **C3,C4** and **D3,D4**). **E.** Fate map using TFAP2α^{IRESCre} shows the location of NC-derived cells in the pharyngeal arches. Note extensive colonization of the mesenchyme between the endodermal pouches (endo) by the TFAP2α^{IRESCre} lineage. αSMA^{+} cells are GFP-negative in Isl1Cre strain (arrows in **C1-C2**). **E2**. αSMA^{+} cells are GFP+ in TFAP2α^{IRESCre} strain. All scale bars are 50 μm. Additional zoom-out views are in Sup. Fig. 6.

FIGURE 8

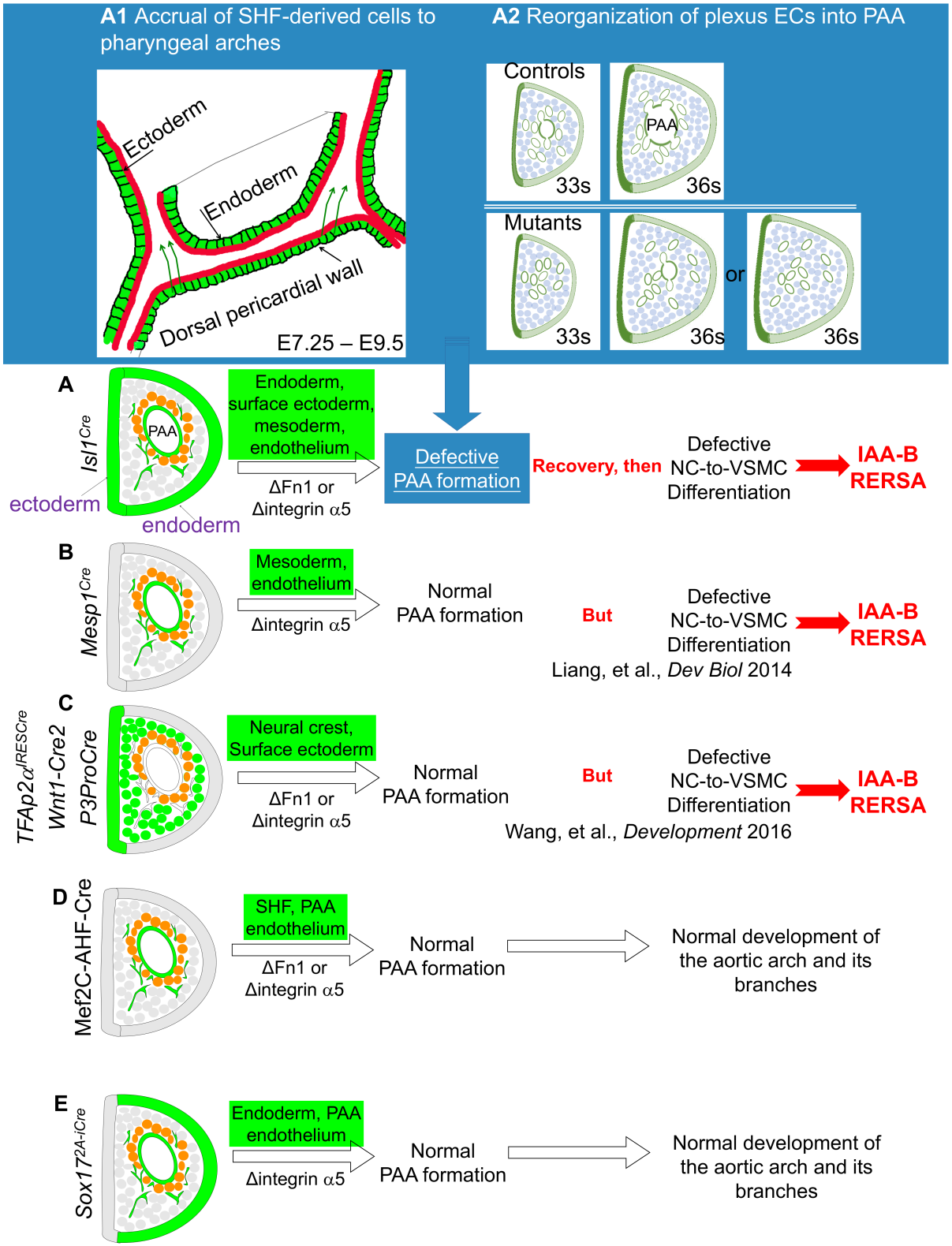

Figure 8. Cell – ECM interactions play essential roles at multiple stages during the development of the aortic arch and its branches. A – E. Depictions of coronal sections through the 4th pharyngeal arch at E10.5. Lineages are marked in green, NC-derived cells are depicted as circles, NC-derived cells next to the PAA endothelium are marked in orange. **A.** The expression of integrin α5β1 and Fn1 in the Isl1 lineages is required for the formation of the 4th PAAs (see **A1** and **A2** in the blue inset) as well as for NC-to-VSMC differentiation. The deletion of integrin α5 or Fn1 in the Isl1 lineages leads to IAA-B and RERSA. **A1 – A2.** Stages during which integrin a5 and Fn1 regulate the 4th PAA formation. **A1.** A schematic of Isl1 lineages (green) in the pharynx at E8.5 – E9.5. Green arrows indicate migration of splanchnic mesoderm cells into the pharyngeal arches. Red lines signify enriched localization of Fn1 protein at germ layer borders. Integrin α5β1 is expressed in all cell types in the pharynx at E8.5 (Chen et al., 2015) and regulates the accrual of pharyngeal mesoderm from the SHF (green arrows). **A2.** During the 10th day of mouse development, integrin α5β1 and Fn1 regulate the remodeling of the plexus endothelium in the 4th pharyngeal arch into the PAA. Isl1 lineages are marked in green. NC-derived cells are in blue. **B.** The expression of integrin α5 in the mesoderm regulates the differentiation of NC-derived cells into VSMCs. The deletion of integrin α5 in Mesp1 lineage, which includes the SHF, leads to defective NC-to-VSMC differentiation and results in the regression of the 4th PAAs leading to IAA-B and RERSA (Liang, et al., *Dev Biol* 2014). **C.** Fn1 becomes upregulated in NC-derived cells adjacent to the 4th PAA ECs between E10.5 and E11.5 The expression of integrin α5β1 and Fn1 in the NC-derived cells is required for NC-to-VSMC differentiation and the stability of the 4th PAA (Wang et al, 2016). The deletion of either integrin α5 or Fn1 in the NC (and the surface ectoderm) leads to IAA-B and RERSA but does not impair PAA formation. **D.** The expression integrin α5 or Fn1 in the SHF is not required for the morphogenesis of the aortic arch and its branches. **E.** The expression of integrin α5 in the endoderm and the pharyngeal endothelia is not required for the development of the aortic arch and its branches.